

CWP-139
DOE/ER14079-27
July 1993



Dynamic Ray Tracing and its Application in Triangulated Media

Andreas Rüger

— Master of Science Thesis —
Geophysics

DISCLAIMER

This report was prepared as an account of work sponsored by an agency of the United States Government. Neither the United States Government nor any agency thereof, nor any of their employees, makes any warranty, express or implied, or assumes any legal liability or responsibility for the accuracy, completeness, or usefulness of any information, apparatus, product, or process disclosed, or represents that its use would not infringe privately owned rights. Reference herein to any specific commercial product, process, or service by trade name, trademark, manufacturer, or otherwise does not necessarily constitute or imply its endorsement, recommendation, or favoring by the United States Government or any agency thereof. The views and opinions of authors expressed herein do not necessarily state or reflect those of the United States Government or any agency thereof.

Center for Wave Phenomena
Colorado School of Mines
Golden, Colorado 80401
303/273-3557

RECORDED
MAY 10 1993

DISTRIBUTION OF THIS DOCUMENT IS UNLIMITED

fpo

ABSTRACT

Hale and Cohen (1991) developed software to generate two-dimensional computer models of complex geology. Their method uses a triangulation technique designed to support efficient and accurate computation of seismic wavefields for models of the earth's interior. Subsequently, Hale (1991) used this triangulation approach to perform dynamic ray tracing and create synthetic seismograms based on the method of Gaussian beams. Here, I extend this methodology to allow an increased variety of ray-theoretical experiments. Specifically, the developed program GBmod (**Gaussian Beam MODeling**) can produce arbitrary multiple sequences and incorporate attenuation and density variations. In addition, I have added an option to perform Fresnel-volume ray tracing (Červený and Soares, 1992). Corrections for reflection and transmission losses at interfaces, and for two-and-one-half-dimensional (2.5-D) spreading are included. However, despite these enhancements, difficulties remain in attempts to compute accurate synthetic seismograms if strong lateral velocity inhomogeneities are present. Here, these problems are discussed and, to a certain extent, reduced. I provide example computations of high-frequency seismograms based on the method of Gaussian beams to exhibit the advantages and disadvantages of the proposed modeling method and illustrate new features for both surface and vertical seismic profiling (VSP) acquisition geometries.

TABLE OF CONTENTS

ABSTRACT	i
ACKNOWLEDGMENTS	iv
Chapter 1 INTRODUCTION	1
Chapter 2 OVERVIEW ON RAY THEORY AND INTRODUCTION TO DYNAMIC RAY TRACING	5
2.1 The Eikonal Equation	5
2.2 Kinematic Ray Tracing Equations	7
2.3 Dynamic Ray-Tracing Equations	9
2.4 Linearizing the Dynamic Ray Tracing Equations	12
2.5 Physical Meaning of \mathbf{Q} and \mathbf{P}	13
2.6 Two- and Two-And-One-Half-Dimensional Models	15
Chapter 3 MODEL REPRESENTATION	21
3.1 Motivation	21
3.2 Reflection and Transmission Sequences	22
3.3 VSP Modeling Experiment	25
Chapter 4 APPLICATION OF DYNAMIC RAY TRACING: RAY DATA AND FRESNEL VOLUMES	33
4.1 Phase-front Curvature and Paraxial traveltimes	33
4.2 Ray Amplitudes	34
4.3 Attenuation	36
4.4 Two-And-One-Half-Dimensional Spreading	39
4.5 Fresnel-Volume Ray Tracing	39
Chapter 5 THE GAUSSIAN BEAM METHOD	43
5.1 Why Do We Use the Gaussian Beam Method?	43
5.2 Gaussian Beam Theory	43
5.3 Difficulties with the Gaussian Beam Approach	47
5.4 Basic Assumptions Inherent to the Beam Approach	53
5.5 Gaussian Beams Across Interfaces	54
5.6 Near-critical Transmission of Gaussian Beams	55
5.7 The Overthrust Model Experiment	58

5.8	Application of Gaussian Beam Modeling In Complex Media	63
5.9	Quo Vadis Gaussian Beams?	67
Chapter 6	CONCLUSION	69
6.1	Summary	69
6.2	Future Work	70
Appendix A	SOLUTION OF THE TWO-DIMENSIONAL DYNAMIC RAY TRACING EQUATIONS	71
Appendix B	MATRIX Q AND ITS RELATION TO THE RAY JACOBIAN	73
Appendix C	TRANSFORMATION OF GAUSSIAN BEAM AMPLITUDES ACROSS INTERFACES	76

ACKNOWLEDGMENTS

Thanks to my advisor Dr. Jack Cohen, Dr. Steve Pruess and Dr. Ken Larner for critiquing and proofreading this thesis and serving in my committee.

Special thanks to my friends Ted Shuck, Lydia Deng, Herman Jaramillo, Norman Ettrich and Michel Dietrich for their support in difficult moments of this research.

I am especially in debts to my wonderful wife Christa, who changed her life to enable my studies here in Golden, Colorado. Without her support, this research would not have been possible.

Financial support for this work was provided in part by the United States Department of Energy, Grant Number DE-FG02-89ER14079. (This support does not constitute an endorsement by DOE of the views expressed in this paper.) Support was also provided by the members of the Consortium Project on Seismic Inverse Methods for Complex Structures at the Center for Wave Phenomena, Colorado School of Mines. I likewise gratefully acknowledge the Fulbright Commission in Bonn, Germany, who honored me with a scholarship for my first year of studies in the United States. The computing facilities necessary for this research are provided by the Center for Geoscience Computing, Colorado School of Mines.

Chapter 1

INTRODUCTION

New triangulation methods for representing subsurface models in computers have helped to overcome limitations inherent in previous computer models of the earth's interior. A mesh of triangles can flexibly characterize complex subsurface models that can, for example, include velocity lenses and overhanging dome structures. Additionally, Hale and Cohen (1991) designed spatial data structures that contain the *adjacency topology* (Weiler, 1988) of the model, so that computing time is not wasted in searching for the triangles and model parameters in the vicinity of an arbitrary point in the model.

The combination of *dynamic ray tracing* (Červený, 1985a) and the triangulation technique is very promising. Dynamic ray tracing is an important extension of the classical kinematic ray tracing. It provides useful dynamic properties such as geometrical spreading and wavefront-curvature information along the rays. Hale (1991) took advantage of the dynamic ray tracing results to generate synthetic seismograms based on the method of Gaussian beams (Červený, et al., 1982).

In this thesis, I present an introduction to the theory of dynamic ray tracing and discuss several applications of this technique. I investigate in detail one specific application, the Gaussian beam method, and address its current limitations.

In the era of high-speed computing, forward modeling based on ray-theoretical methods competes with finite-difference approaches (e.g., Fei, 1993). The latter allows specification of model parameters such as the seismic velocity at each point in the gridded model. If the grid spacing is chosen fine enough, the accuracy of the calculated synthetic seismograms is very good and synthetic sections generated with a finite-difference method provide all types of seismic events simultaneously. However, this often makes it difficult to identify reflections from interfaces of interest. Moreover, the computing speed of finite-difference methods is about two orders of magnitude slower than for ray tracing experiments. This significantly reduces the application of finite-difference methods as an interpretation tool.

If certain requirements are met, ray-theoretical techniques and, in particular, the dynamic ray-tracing method do have a future in seismic modeling. Several criteria may be established to compare the performance of either method (see Table 1.1). Here, based on my experience, I assign subjective grades from 1 to 10 to the performance of finite difference methods (**FD**), Hale's Gaussian beam modeling package (**oldGBmod**) and its extension (**newGBmod**), which I introduce in this paper.

- **Flexibility :** The first criterion assesses the model complexity and the variety of ray modes that can be traced. I have added an option to specify an attenuation factor and density for each geologic block, i.e., for each area bounded by interfaces. Moreover, the software now allows the introduction of a broader class of raypaths.

Table 1.1. A comparison of finite-difference methods (**FD**), Hale's Gaussian beam modeling package (**oldGBmod**) and its extension (**newGBmod**), which is introduced in this paper. Details are given in the text.

That is, as shown in Figure 1.1, interfaces no longer are limited to being either reflectors or transmitters of seismic energy, but now can be both, in a specified sequence. This generalization broadens the applicability of the modeling. For example, it is now possible to include multiples.

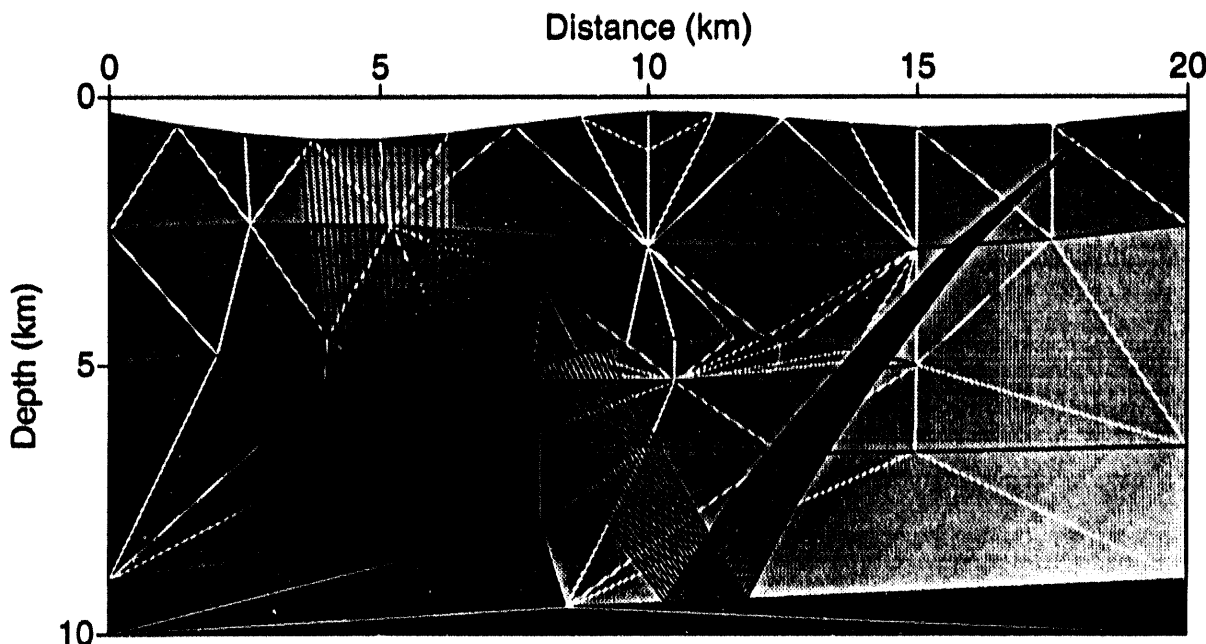


FIG. 1.1. Ray tracing in a complex subsurface model. This model includes sharp-edged interfaces and lens-type structures. Lithological interfaces are represented by black lines. The shading denotes the seismic velocity field. Also shown as black lines are raypaths corresponding to one type of interface multiple. The white lines are edges of auxiliary triangles used in the model building.

- **Diagnostics :** The second criterion evaluates the capability of the method to act as a tool for interpretation and understanding of wave propagation in complex structures. Several new options have been included and will be presented in this paper. One of the new features, called *physical ray tracing* or *Fresnel-volume ray tracing* (Červený and Soares, 1992), may be used to study the resolution and the validity conditions of the ray method.
- **Accuracy :** Third, accurate seismograms have to be computed. The computation of the reflection and transmission losses at interfaces as well as correction for 2.5-D amplitude spreading improve the accuracy of the Gaussian beam ray tracing. However, problems remain when dealing with significant inhomogeneities in the

model. Some limitations are intrinsic to ray methods; others are specific to the Gaussian beam approach. Both are discussed later in this paper.

- **Speed :** The fourth criterion, computational aspects, underlines one of the big advantages of ray methods. The new options of the ray-tracing package such as the computation of the out-of-plane spreading, energy partitioning at interfaces, and attenuation, can be performed while still maintaining the attractive feature of computational efficiency with limited computer storage requirements.

To better understand the advantages and disadvantages of dynamic ray tracing, I illustrate the new options for both surface and VSP acquisition geometries. A comparison with VSP data obtained in a physical modeling laboratory supports benefits of the ray-theoretical modeling.

Modeling using the Gaussian beam method is only one possible application of the dynamic ray-traced data generated along the ray. Alternative methods (e.g., the paraxial methods) can also use these data to create synthetic seismograms. The new modifications to the program GBmod, such as the tracing of multiples, computation of out-of-plane spreading, or reflection and transmission correction are evaluated independently of the Gaussian beam procedure.

Chapter 2

OVERVIEW ON RAY THEORY AND INTRODUCTION TO DYNAMIC RAY TRACING

This chapter gives an introduction to various aspects of ray theory. Although most of the derivations can be found in textbooks (e.g., Aki and Richards, 1980), I decided to go into some detail whenever it seemed necessary. My goal is to explain this fascinating theory in such a way that students and scientists from neighboring disciplines can follow, or even better, find interest in the combination of physics and mathematics presented.

As a starting point, I first consider an isotropic, perfectly elastic inhomogeneous medium in three dimensions. Later I decrease the complexity towards our needs for the modeling program. In the following derivations, if not stated otherwise, I make use of rectangular cartesian coordinates with the notation x_i , with $i = 1, 2, 3$.

2.1 The Eikonal Equation

Solving the eikonal equation by the method of characteristics provides a mathematical derivation of the ray tracing equations for determining the ray path and the properties of the wavefront traveling along the ray. Other derivations based on energy considerations or on variational calculus such as Fermat's principle often offer a better physical insight; however, they must be applied to longitudinal and shear waves separately. This separation cannot be performed in the general case, and strictly holds only for homogeneous media.

To study the raypath, the amplitudes and the shape of the wavefront propagating along a ray, it is therefore useful to start with the *elastodynamic equation of motion*.

$$\sigma_{ij,j} = \rho u_{i,tt}, \quad (2.1)$$

where u_i and σ_{ij} denote the cartesian components of the displacement field and the stress tensor, respectively. As throughout this thesis, the Einstein summation convention is used. Moreover, we use a commonly accepted notation for the partial derivatives with respect to cartesian components x_i and time t , e.g. $\sigma_{ij,j} = \frac{\partial \sigma_{ij}}{\partial x_j}$, $u_{i,tt} = \frac{\partial^2 u_i}{\partial t^2}$. ρ is the density of the medium. As shown in the literature (e.g., Aki and Richards, 1980), the isotropic stress tensor can be expressed in terms of u_i and the Lamé constants λ and μ as follows:

$$\sigma_{ij} = \lambda \delta_{ij} u_{k,k} + \mu(u_{i,j} + u_{j,i}), \quad (2.2)$$

where δ_{ij} denotes the Kronecker-delta symbol:

$$\delta_{ij} \equiv \begin{cases} 1 & \text{if } i = j \\ 0 & \text{if } i \neq j \end{cases}$$

One possible trial solution of the elastodynamic equation of motion is motivated by the solution of the homogeneous case and has the form

$$u_k(\omega, x_i) = e^{-i\omega(t - \tau(x_i))} \sum_{n=0}^{\infty} U_k^{(n)}(x_i) \left(\frac{1}{-i\omega}\right)^n. \quad (2.3)$$

We could also use an equivalent time-domain approach, but this form of *ansatz* in the frequency domain is conceptually simpler, especially if we consider the medium properties such as density and Lamé constants to be independent of time. Note that only the amplitude coefficients $U_k^{(n)}$ and the eikonal τ depend on spatial coordinates. This ray series solution is written in inverse powers of frequency ω . If we are interested in the high frequencies, we need only consider the first few terms in the series. Specifically, in practical applications such as our modeling, only the $n = 0$ term is used. In this case, $U_k^{(0)}$ will be called U_k . If we are interested in higher-order waves, more than the $U_k^{(0)}$ term is needed. The best known example of such is probably the head-wave. Its first non-vanishing amplitude coefficient is $U_k^{(1)}$. A detailed discussion for the interested reader may be found in Červený and Ravindra (1971) and Bleistein (1984). A simple, but tedious, substitution of (2.3) and (2.2) into the equation of motion (2.1) will lead to the eikonal equation and transport equation. After rearranging the result in expressions with the same powers of $(i\omega)$, we obtain the basic system of equations for the ray method:

$$0 = (i\omega)^2 N_i(U_j) + (i\omega) M_i(U_j) + O(1),$$

where $N_i(U_j) \equiv U_j ((\lambda + \mu)\tau_{,i}\tau_{,j} + \mu\delta_{ij}\tau_{,k}\tau_{,k} - \rho\delta_{ij});$

$$M_i(U_j) \equiv (\lambda + \mu)(\tau_{,i}U_{j,j} + \tau_{,j}U_{j,i} + U_j\tau_{,ij}) + \mu(2\tau_{,j}U_{i,j} + U_i\tau_{,jj}) + \lambda_{,i}\tau_{,j}U_j + \mu_j(\tau_{,j}U_i + \tau_{,i}U_j).$$

To solve for τ and U_i independent of frequency, we must solve the following two equations:

$$N_i(U_j) = 0, \quad (2.4)$$

$$M_i(U_j) = 0. \quad (2.5)$$

Equation (2.4) can be identified as an eigenvalue problem with three mutually orthogonal eigenvectors. Two of these eigenvectors correspond to two identical eigenvalues and span a plane orthogonal to the ray. The third eigenvector is polarized parallel to the ray.

Analytical expressions can be found for the eigenvalues and lead to the eikonal

equation for each wavetype:

$$\begin{aligned}\tau_{,i}\tau_{,i} &= \left(\frac{1}{v_s}\right)^2, \\ \tau_{,i}\tau_{,i} &= \left(\frac{1}{v_p}\right)^2.\end{aligned}\quad (2.6)$$

$v_s = \sqrt{\frac{\mu}{\rho}}$ represents the seismic velocity of the wavetype polarized perpendicular to the ray and $v_p = \sqrt{\frac{2\mu+\lambda}{\rho}}$ the velocity of the wave polarized parallel to the ray. Thus, in isotropic, inhomogeneous media, high frequency wavefields can be decoupled into two independently traveling wavetypes.

A more detailed discussion on the derivation of the eikonal equation is provided, for example, in Cervený (1987). Equation (2.5) will be used to evaluate the amplitude of the wave.

2.2 Kinematic Ray Tracing Equations

The mathematical, straightforward way to derive the solution of the eikonal equation is called the *method of characteristics*.

$$\tau(x_j)_{,i} \tau(x_j)_{,i} = \frac{1}{v^2(x_j)}$$

is a first order, non-linear partial differential equation of the Hamilton-Jacobi type. We can rewrite the equation as

$$\frac{1}{n} \left((\tau_{,i} \tau_{,i})^{\frac{n}{2}} - \frac{1}{v^n} \right) = 0. \quad (2.7)$$

If we introduce the *slowness vector* p_i :

$$p_i \equiv \tau_{,i} \quad ; \quad |p| = \frac{1}{v},$$

the Hamilton-Jacobi equation takes the form

$$H(p_i, x_i) = \frac{1}{n} (p_i p_i)^{n/2} - \left(\frac{1}{v}\right)^n = 0. \quad (2.8)$$

Using the method of characteristics (e.g., Bleistein, 1984), we obtain the following equations, which are called the *ray trace equations*:

$$\frac{du}{d\tau} = v^n d\tau, \quad (2.9)$$

$$\frac{dx_i}{du} = p_i \frac{1}{v^{n-2}}, \quad (2.10)$$

$$\frac{dp_i}{du} = -\frac{1}{v^{n+1}} \frac{\partial v}{\partial x_i}. \quad (2.11)$$

The solution of equations (2.10) and (2.11) represents the trajectory x_i and the distribution of p_i along the ray as a function of a monotonically increasing independent variable u . The solution $x_i(u)$ is called the *raypath*. Note that we are free to choose n . If we set n equal to zero, then u is the travelttime τ along the ray. If we assign to n the value 1, (2.9) is of the form:

$$du = v d\tau = ds.$$

Here, s is called the arclength along the ray. s is measured from some reference point on the ray. However, (2.9) suggests that the simplest form can be achieved by setting n equal to 2. For this specification, we follow Bleistein (1984) and set

$$du = v^2 d\tau = d\sigma. \quad (2.12)$$

The nonphysical quantity σ has units of $[\frac{\text{length}^2}{\text{time}}]$. The ray trace system may now be written in the convenient form:

$$\begin{aligned} \frac{dx_i}{d\sigma} &= p_i, \\ \frac{dp_i}{d\sigma} &= \frac{1}{2}(\frac{1}{v^2})_{,i}, \\ \frac{d\tau}{d\sigma} &= v^{-2}. \end{aligned} \quad (2.13)$$

The first equation in (2.13) does not contain any velocity dependence. As a consequence, we are able to find simple analytic expressions for rays in some special situations. For example, if the gradient of v^{-2} in the medium is constant, we can solve for the slowness components p_i analytically. The inverse of the velocity squared, the *sloth*, can then be written in the form

$$\frac{1}{v^2} \equiv s(x, z) = s_{00} + s_{,i} x_i,$$

and the equation for the slowness vector yields:

$$p_i(\sigma) = p_i(\sigma_0) + \frac{1}{2}s_{,i}(\sigma - \sigma_0).$$

Using this equation, we can write for the coordinates and the travelttime along the raypath the following expressions:

$$\begin{aligned} x_i(\sigma) &= x_i(\sigma_0) + p_i(\sigma_0)(\sigma - \sigma_0) + \frac{1}{4}s_{,i}(\sigma - \sigma_0)^2 \\ \tau(\sigma) &= \tau(\sigma_0) + [s_{00} + s_{,i}x_i(\sigma_0)](\sigma - \sigma_0) \\ &\quad + \frac{1}{2}[s_{,i}p_i(\sigma_0)](\sigma - \sigma_0)^2 \\ &\quad + \frac{1}{12}[s_{,i}^2](\sigma - \sigma_0)^3. \end{aligned} \quad (2.14)$$

The simplicity of the solutions and the fact that polynomials required to get slowness

and traveltimes can be evaluated very efficiently on the computer, make media with a constant gradient in slope very attractive.

This approach to solving for the slowness distribution and the raypath lacks direct physical justification. However, the Hamilton-Jacobi equation (2.8) can also be derived by applying classical mechanics theory (e.g., Goldstein, 1950, Chapter 9). Considering the propagation of waves as movement of particles also leads to an expression equivalent to the eikonal equation. In this sense, ray theory is only a classical-mechanics approximation of wave propagation. Therefore, observations obtained by using the ray-theoretical approach outlined in this chapter are only valid if effects involving the wavelength of the signal are negligible. This is the physical basis of the well-known restriction (see Bleistein, 1984) that the length scale of the medium must be much larger than the wavelength of the signal.

2.3 Dynamic Ray-Tracing Equations

The system of equations (2.13) can be used to evaluate slowness and traveltimes along a raypath. In this chapter, however, we advance one step further and try to compute properties of the wavefield close to the ray. The cartesian coordinate system is not very convenient for this application. Better suited are orthogonal coordinate systems that move along the ray and whose basis vectors coincide with the polarisation vectors of P and S waves. Such systems are described by Červený and Hron (1980) or Hubral (1980), and have been used to investigate geometrical spreading and curvature along the ray.

For each ray, we introduce an orthogonal curvilinear coordinate system (q_1, q_2, s) connected to the ray. In this so-called *ray-centered coordinate system*, the coordinate s represents the monotonically increasing arclength along the ray. Parameters q_1 and q_2 form a 2-D cartesian coordinate system in a plane orthogonal to the ray at fixed arclength. As sketched in Figure 2.1, the basis vectors are the unit tangent \hat{t} to the ray at given s and the unit vectors \hat{e}_1 and \hat{e}_2 perpendicular to the ray. They can be computed by making use of the normal and binormal to the ray at fixed s and by integrating over the torsion of the ray trajectory.

Any radius vector r_i from the origin 0 of the coordinate system $(q_1 = q_2 = 0, s = s_0)$ to a point S in the vicinity of the ray can now be expressed in the form:

$$\bar{r}(q_1, q_2, s) = \bar{r}(0, 0, s) + q_1 \hat{e}_1(s) + q_2 \hat{e}_2(s).$$

The vector basis $(\hat{e}_1, \hat{e}_2, \hat{t})$ is right-handed. The scale factors for this curvilinear coordinate system are:

$$h_{q_1} = h_{q_2} = 1, \quad h_s = h,$$

where h is given by:

$$h = 1 + q_1 \left(v^{-1} \frac{\partial v}{\partial q_1} \right)_{q_1=q_2=0} + q_2 \left(v^{-1} \frac{\partial v}{\partial q_2} \right)_{q_1=q_2=0}.$$

If we define capital letter indices to have the values 1 and 2, we can rewrite this equation

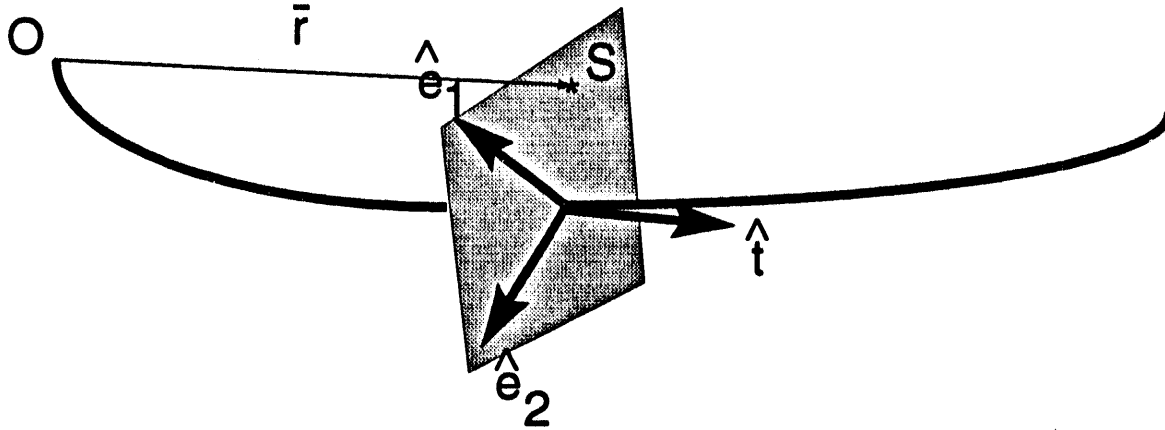


FIG. 2.1. The ray-centered coordinate system in 3-D uses as basis vectors the unit tangent \hat{t} to the ray at given s and the unit vectors \hat{e}_1 and \hat{e}_2 perpendicular to the ray.

as:

$$h = 1 + q_I \left(v^{-1} \frac{\partial v}{\partial q_I} \right)_{q_K=0}. \quad (2.15)$$

We are now prepared to express the earlier-derived eikonal equation (2.10) in ray-centered coordinates:

$$(\nabla \tau)^2 = \left(\frac{\partial \tau}{\partial q_1} \right)^2 + \left(\frac{\partial \tau}{\partial q_2} \right)^2 + \frac{1}{h^2} \left(\frac{\partial \tau}{\partial s} \right)^2 = \frac{1}{v^2(q_1, q_2, s)}. \quad (2.16)$$

It is our intention to approximate the wavefront or the traveltime field close to a selected *central* ray. In the ray-centered coordinate system this involves only a Taylor expansion in the \hat{e}_1 and \hat{e}_2 directions. We will expand our expressions up to the second order in q_1 and q_2 . Hence, the results of our computations are exact only at the central ray itself, and the approximation holds for only small values of q_1 and q_2 . To facilitate the next derivations, some commonly-used notation (e.g. Červený [1987]) is introduced.

$$\begin{aligned} v(s) &= [v(q_1, q_2, s)]_{q_K=0}, \\ v_I(s) &= \left[\frac{\partial v(q_1, q_2, s)}{\partial q_I} \right]_{q_K=0}, \\ v_{IJ}(s) &= \left[\frac{\partial^2 v(q_1, q_2, s)}{\partial q_I \partial q_J} \right]_{q_K=0}. \end{aligned}$$

For fixed arclength, the Taylor expansion of the velocity field close to a central ray is

$$v(q_1, q_2, s) \approx v(s) + v_{,K} q_K + \frac{1}{2} v_{,KL} q_K q_L.$$

After multiplying by h^2 and expanding to second order in q_1 and q_2 , (2.16) takes the form

$$h^2 \left[\left(\frac{\partial \tau}{\partial q_1} \right)^2 + \left(\frac{\partial \tau}{\partial q_2} \right)^2 \right] + \left(\frac{\partial \tau}{\partial s} \right)^2 = \frac{1}{v^2(s)} - \frac{1}{v^3(s)} v_{,KL} q_K q_L. \quad (2.17)$$

Equation (2.17) describes the traveltime field in the paraxial vicinity of the ray up to the second order in q_1 and q_2 . The solution $\tau(q_1, q_2, s)$ can be expressed as a Taylor series in q_1 and q_2 .

$$\tau(q_1, q_2, s) = \tau(0, 0, s) + \frac{1}{2} q_I q_J M_{IJ}. \quad (2.18)$$

Here we denote the symmetric matrix of second derivatives of the traveltime field by $\mathbf{M}(\mathbf{s})$.

$$M_{IJ}(s) = \left[\frac{\partial^2 \tau(q_1, q_2, s)}{\partial q_I \partial q_J} \right]_{q_K=0}.$$

The Taylor expansion of $\tau(q_1, q_2, s)$ does not include a linear term $(\frac{\partial \tau(q_1, q_2, s)}{\partial q_I})_{q_K=0}$ because wavefronts are orthogonal to rays in isotropic media. However, outside the central ray, we find from equation (2.18) that

$$\begin{aligned} \frac{\partial \tau(q_1, q_2, s)}{\partial q_I} &= M_{IK} \cdot q_K, \\ \frac{\partial \tau(q_1, q_2, s)}{\partial s} &= \frac{\partial \tau(0, 0, s)}{\partial s} + \frac{1}{2} q_I q_J \cdot \frac{dM_{IJ}}{ds}. \end{aligned}$$

These relations are inserted in (2.17) and the assumption is made that h^2 is close to unity, i.e.,

$$q_I \cdot \left(v^{-1} \frac{\partial v}{\partial q_I} \right)_{q_K=0} \ll 1. \quad (2.19)$$

Equation (2.19) defines the paraxial vicinity of the ray. Under this assumption, the paraxial approximation of the eikonal equation in ray-centered coordinates reduces to the simple equation

$$\frac{d\mathbf{M}}{ds} + v\mathbf{M}^2 + \frac{1}{v^2} \mathbf{V} = \mathbf{0}, \quad (2.20)$$

or, if we choose σ (see equation (2.12)) as the monotonically increasing parameter along the ray:

$$\frac{d\mathbf{M}}{d\sigma} + \mathbf{M}^2 + \frac{1}{v^3} \mathbf{V} = \mathbf{0}, \quad (2.21)$$

where

$$\mathbf{V} = V_{IJ}(\sigma) = \left[\frac{\partial^2 v(q_1, q_2, \sigma)}{\partial q_I \partial q_J} \right]_{q_K=0}$$

is the matrix of second derivatives of the velocity field at points along the ray under investigation. Equation (2.21), the so-called dynamic ray tracing equation, is a first-

order differential equation that must be solved along a known ray. This equation is a nonlinear Riccati-type differential equation and has no closed-form solution.

2.4 Linearizing the Dynamic Ray Tracing Equations

To facilitate the procedure of solving the Riccati equation, several authors (e.g., Červený and Hron [1980]) proposed two substitutions to obtain a new set of linear differential equations of first-order. Following their lead, we eliminate the nonlinear term by setting

$$\mathbf{M}(\sigma) = \frac{d\mathbf{Q}}{d\sigma} \mathbf{Q}^{-1}. \quad (2.22)$$

Introducing the (2×2) -matrix $\mathbf{P} = \frac{d\mathbf{Q}}{d\sigma}$, one obtains a set of eight linear, first-order differential equations

$$\frac{d\mathbf{Q}}{d\sigma} = \mathbf{P} \quad ; \quad \frac{d\mathbf{P}}{d\sigma} = -\frac{1}{v^3} \mathbf{V} \mathbf{Q}. \quad (2.23)$$

If we define matrices \mathbf{X} and \mathbf{S} by

$$\mathbf{X} = \begin{pmatrix} Q_{11} & Q_{12} \\ Q_{21} & Q_{22} \\ P_{11} & P_{12} \\ P_{21} & P_{22} \end{pmatrix} \quad \mathbf{S} = \begin{pmatrix} 0 & 0 & 1 & 0 \\ 0 & 0 & 0 & 1 \\ -\frac{1}{v^3} v_{,11} & -\frac{1}{v^3} v_{,12} & 0 & 0 \\ -\frac{1}{v^3} v_{,21} & -\frac{1}{v^3} v_{,22} & 0 & 0 \end{pmatrix},$$

then equation (2.23) can be represented in the form

$$\frac{d}{d\sigma} \mathbf{X} = \mathbf{S} \mathbf{X}. \quad (2.24)$$

Both columns of \mathbf{X} must satisfy the same set of equations, in other words, we must only solve one system of four differential equations twice with different initial conditions.

The solution space of a system of the form

$$\frac{d}{d\sigma} \mathbf{Y} = \mathbf{S} \mathbf{Y},$$

with \mathbf{Y} being a (4×1) matrix, is spanned by four linearly independent solution vectors. If we solve the system for four linearly independent intrinsic initial choices of $\mathbf{Y}(\sigma_0)$ as, for example,

$$\{\mathbf{Y}^1(\sigma_0), \mathbf{Y}^2(\sigma_0), \mathbf{Y}^3(\sigma_0), \mathbf{Y}^4(\sigma_0)\} = \left\{ \begin{pmatrix} 1 \\ 0 \\ 0 \\ 0 \end{pmatrix}, \begin{pmatrix} 0 \\ 1 \\ 0 \\ 0 \end{pmatrix}, \begin{pmatrix} 0 \\ 0 \\ 1 \\ 0 \end{pmatrix}, \begin{pmatrix} 0 \\ 0 \\ 0 \\ 1 \end{pmatrix} \right\},$$

then the solution space is determined. For convenience, the four solution vectors are grouped together as columns of the *fundamental* matrix $\Pi(\sigma_0, \sigma)$. Every solution $\mathbf{W}(\sigma)$ can now be computed by a simple matrix multiplication of Π with a (4×1) matrix $\mathbf{C}(\sigma_0)$

of specific initial conditions:

$$\mathbf{W}(\sigma) = \Pi(\sigma_0, \sigma) \cdot \mathbf{C}(\sigma_0) .$$

Thus, as soon as $\Pi(\sigma_0, \sigma)$ is known, we can find solutions of the dynamic ray tracing system analytically for any initial condition specified at σ_0 , without repeating the dynamic ray tracing.

This is the general formulation of dynamic ray tracing. However, our focus of attention is not the most general three-dimensional case. We make use of (2.23) as a starting point to investigate the behavior of some important physical quantities in more restricted media.

2.5 Physical Meaning of \mathbf{Q} and \mathbf{P}

Before we start to interpret the meaning of \mathbf{Q} and \mathbf{P} , we should recall the three important coordinate systems used in the derivations. This choice of coordinates, as seen in Figure (2.2), will be applied throughout the following sections.

- Cartesian coordinates x_i
- Ray coordinates $\gamma_i = (\gamma_1, \gamma_2, \gamma_3 = \sigma)$. $\gamma_I = (\gamma_1, \gamma_2)$ may be identified as the takeoff angle and the azimuth of the ray at an initial point and specify a ray in a three-dimensional medium. The monotonically increasing parameter along the ray, σ , can be evaluated using

$$\sigma = \sigma_0 + \int_{\tau_0}^{\tau} v^2 d\tau = \sigma_0 + \int_{s_0}^s v ds.$$

- Orthogonal ray-centered coordinates $q_i = (q_1, q_2, q_3 = s)$ along the ray. q_1 and q_2 span a cartesian coordinate system perpendicular to the ray at fixed arclength s .

So far, the matrices \mathbf{P} and \mathbf{Q} appear as mathematical, abstract quantities. However, Červený (1987) shows that they have associated physical meanings. Specifically, if at any point of the ray, the (2×2) matrices \mathbf{P} and \mathbf{Q} are initialized as the transformation matrices from ray parameters to ray-centered components of the slowness vector and from ray parameters to ray-centered coordinates, then they will represent these transformation matrices as long as the velocity varies continuously:

$$\mathbf{Q}(\sigma) = \left[\frac{\partial q_I}{\partial \gamma_J} \right]_{q_K=0} , \quad \mathbf{P}(\sigma) = \left[\frac{\partial p_I}{\partial \gamma_J} \right]_{q_K=0} . \quad (2.25)$$

It is worthwhile to emphasize the meaning of the matrix elements of \mathbf{P} and \mathbf{Q} . For example, according to the first equation in (2.25), Q_{11} is the change of the trajectory in the q_1 direction for a infinitesimal variation $\delta\gamma_1$ in the takeoff angle. This change is measured perpendicular to the unperturbed ray in the \hat{e}_1 direction. Similarly, P_{12} is the change of the first component of the slowness vector due to an infinitesimal change in

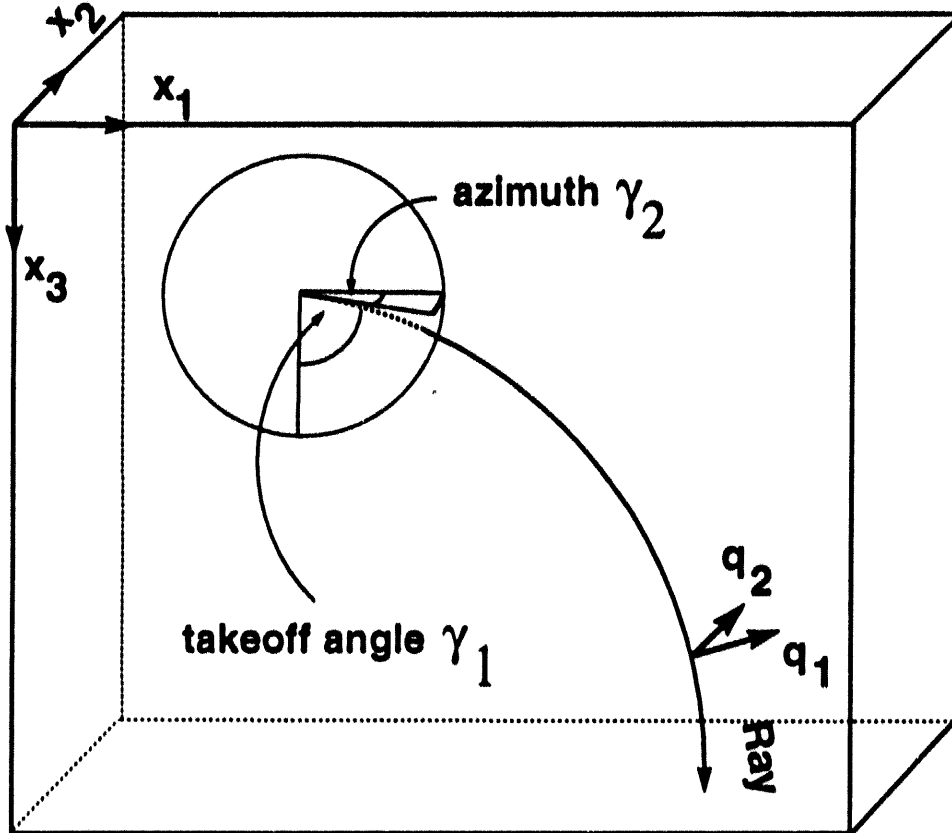


FIG. 2.2. Our specific choices of coordinate systems. q_1 and q_2 correspond to the ray-centered coordinate system, γ_1 and γ_2 are the ray coordinates. x_1 , x_2 and x_3 represent the cartesian coordinate frame.

azimuth and so on. In the next section, these meanings are illustrated and discussed in more detail.

Once \mathbf{P} and \mathbf{Q} are evaluated along the ray, they can be used to compute additional physical properties along the ray. Recalling the introduction of both matrices (2.22), it is straightforward to show how the matrix of second derivatives of the travelttime field \mathbf{M} is obtained. In a similar manner, the (2×2) matrices \mathbf{K} and \mathbf{R} of curvature and radii of curvature of the wavefront are computed.

$$\begin{aligned}\mathbf{M} &= \frac{d\mathbf{Q}}{d\sigma} \cdot \mathbf{Q}^{-1}, \\ \mathbf{K} &= v(\sigma) \cdot \mathbf{M}, \\ \mathbf{R} &= \mathbf{K}^{-1}.\end{aligned}$$

2.6 Two- and Two-And-One-Half-Dimensional Models

A significant simplification can be achieved by considering a two dimensional model. One ray coordinate and the initial point is now sufficient to define a ray, and any point S close to a ray can be described by two ray-centered coordinates. This situation is sketched in Figure 2.3.

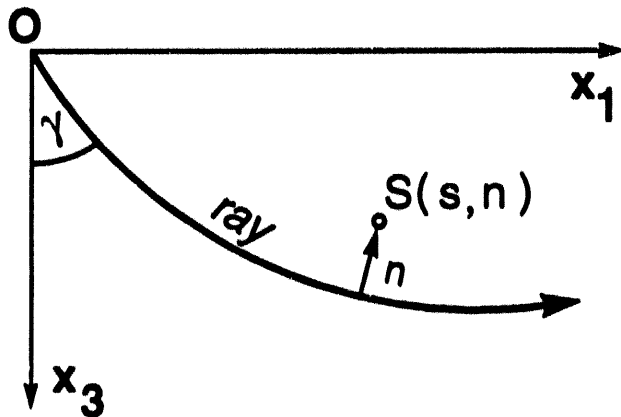


FIG. 2.3. A ray in a 2D-medium is well defined by a starting point O and one ray coordinate. Here this coordinate is chosen to be the takeoff angle. Any point S close to the ray is a function of the ray-centered coordinate s and the distance perpendicular to the ray n .

In this 2-D case, \mathbf{Q} and \mathbf{P} are reduced to simple scalars q and p because all derivatives with respect to q_2 and γ_2 vanish. The dynamic ray tracing system (2.23) reduces to only two linear, ordinary differential equations:

$$\frac{dq}{d\sigma} = p \quad , \quad \frac{dp}{d\sigma} = -\frac{1}{v^3} v_{,11} q . \quad (2.26)$$

Whenever the gradient of v^{-2} in the medium is constant, this system has analytic solutions, which are shown explicitly in Appendix A or in Hale (1991).

There is one severe disadvantage in using the 2-D approach. The elimination of the second out-of-plane coordinate implicitly introduces an infinite extension of the physical properties of the source in the x_2 direction. The point source is thereby converted into a line source which generates cylindrical wavefronts. The geometrical spreading and phase behavior of cylindrical waves differs significantly from those due to a point source. The amplitude difference can be removed by considering a three-dimensional medium with lateral and vertical velocity variations restricted to a specified plane. No velocity variation is allowed in the direction normal to this plane. This situation, as illustrated in Figure 2.4,

is referred to as *two-and-one-half dimensional*. Any ray with its initial slowness vector in the (x_1, x_3) plane will stay in this plane. Thus, except for the three-dimensional spreading, the problem of interest is essentially two-dimensional. Two excellent papers on this subject are Bleistein (1986) and Docherty (1987). The geologic interpretation of this situation is a seismic experiment carried out in the dip direction. It is obvious that derivatives of the velocity field with respect to q_2 are zero if the basis vector \hat{e}_2 of Figure 2.1 points in the x_2 direction.

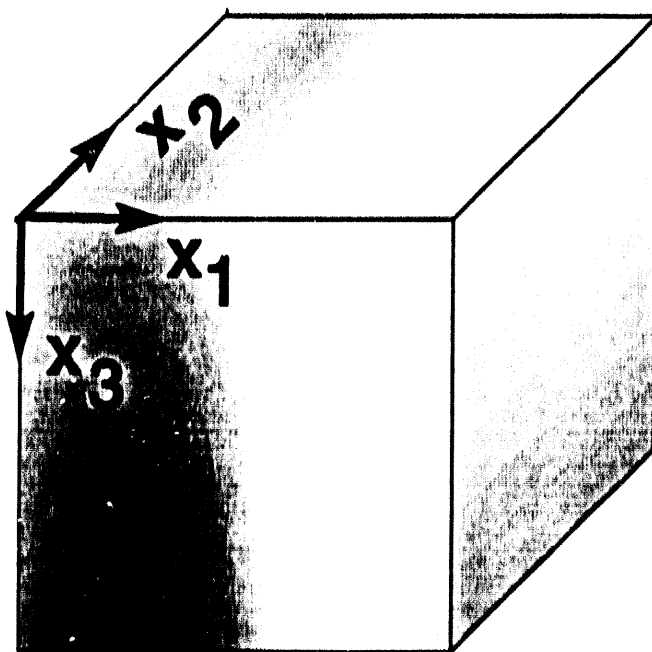


FIG. 2.4. Example of a common-strike medium. Dark shading denotes a high seismic wave velocity. The velocity field may only change in x_1 and x_3 direction, with no velocity changes in the x_2 direction. Any ray with its initial slowness vector in the (x_1, x_3) plane will stay in this plane. Thus, except for the three-dimensional spreading, the problem of interest is essentially two-dimensional. This situation is referred to as *two-and-one-half dimensional*.

Equation (2.23) reduces significantly for the 2.5 D case.

$$\begin{aligned}\frac{\partial Q_{11}}{\partial \sigma} &= P_{11} & \frac{\partial P_{11}}{\partial \sigma} &= -\frac{1}{v^3} v_{,11} Q_{11} \\ \frac{\partial Q_{12}}{\partial \sigma} &= P_{12} & \frac{\partial P_{12}}{\partial \sigma} &= -\frac{1}{v^3} v_{,11} Q_{12} \\ \frac{\partial Q_{22}}{\partial \sigma} &= P_{22} & \frac{\partial P_{22}}{\partial \sigma} &= 0 \\ \frac{\partial Q_{21}}{\partial \sigma} &= P_{21} & \frac{\partial P_{21}}{\partial \sigma} &= 0\end{aligned}\tag{2.27}$$

Let us put a point source into this medium. The choice of coordinates is the same as that sketched in Figure (2.2). Imagine a ray that starts with the initial slowness vector perpendicular to the x_2 axis. This ray will stay in a plane perpendicular to the x_2 axis because there are no changes of velocity in the x_2 direction. This also implies that \hat{e}_2 always points in the out-of-plane direction. Now, we infinitesimally vary the ray coordinates and consider the values of our transformation matrices \mathbf{Q} and \mathbf{P} at the source itself. Q_{11} is the change of the trajectory in the q_1 direction for a infinitesimal variation $\delta\gamma_1$ in the takeoff angle. Because we deal with a *point* source, we certainly will not find any offset δq_1 at the source itself. The same argument holds for all elements Q_{IJ} . On the other hand, the direction of the ray and thus the slowness vector are obviously functions of $\delta\gamma_1$ and $\delta\gamma_2$. The change of the first ray-centered component of the slowness vector by varying the takeoff angle by $\delta\gamma_1$ is $\delta p_1 = \frac{1}{v(\sigma_0)} \delta\gamma_1$. Similarly we can get P_{22} . However, if we change the azimuth, we do not get any change in the first component. The same is true for of variations of the takeoff angle on the p_2 component. In summary, we find:

$$\begin{aligned}Q_{IJ}(\sigma_0) &= 0; \\ P_{12}(\sigma_0) &= 0; \\ P_{21}(\sigma_0) &= 0; \\ P_{11}(\sigma_0) &= \frac{1}{v(\sigma_0)}; \\ P_{22}(\sigma_0) &= \frac{1}{v(\sigma_0)} \sin\gamma_1.\end{aligned}\tag{2.28}$$

To verify these results qualitatively, we can compute the matrix of curvature at the point source $\mathbf{K}(\sigma_0)$.

$$\mathbf{K}(\sigma_0) = v(\sigma_0) \cdot \mathbf{P}(\sigma_0) \mathbf{Q}^{-1}(\sigma_0) \rightarrow \infty.$$

As expected, we find infinite curvature of the wavefront at the source.

Applying the initial conditions, (2.28) reduces the system (2.27) to two equations: Clearly, the set of equations for Q_{21} and P_{21} yields the solutions $Q_{21}(\sigma) = 0$ and $P_{21}(\sigma) = 0$. The same, though less obvious, is true for Q_{12} and P_{12} . This set represents a homogeneous system with zero initial conditions. Simple integration helps to solve for Q_{22} and P_{22} .

$$\begin{aligned}
 P_{22}(\sigma) &= P_{22}(\sigma_0), \\
 Q_{22}(\sigma) &= \int_{\sigma_0}^{\sigma} P_{22}(\sigma') d\sigma' , \\
 &= P_{22}(\sigma_0) (\sigma - \sigma_0).
 \end{aligned} \tag{2.29}$$

The solution for Q_{11} and P_{11} is the same as for the two-dimensional case. In other words, if we have available a routine which evaluates the dynamic ray-trace equation in two dimensions; then a simple computation for Q_{22} solves our two-and-a-half-dimensional problem for a point source. Specifically, this correction can be easily introduced if we use σ as our monotonically increasing parameter along the ray. A similar discussion can be found in Červený (1987).

As shown in Chapter 4, the above derived properties of the 2.5-D dynamic ray tracing imply the same out-of-plane spreading correction for the ray amplitudes as that derived by Bleistein (1986).

Chapter 3

MODEL REPRESENTATION

The triangulation method for constructing and representing subsurface models is mainly built upon the research of Hale and Cohen (1991). In order to trace a broader variety of ray modes and to allow VSP experiments, I develop a more dynamic way to defining interfaces than in the previous approach. In this chapter, after giving some motivation for using the triangulation method, I describe and illustrate the new modifications to the program GBmod.

3.1 Motivation

There exist a variety of methods to represent geologic subsurface models in the computer. One possibility would be to introduce a uniform rectangular-grid sampling of subsurface parameters such as the speed of seismic waves. To understand the behavior of physical phenomena, such as the propagation of sound in the subsurface, one has to apply a mathematical operator on this grid. This approach of *finite-differencing* the wavefield is inefficient and may involve millions of floating point calculations. Less cost effective is the numerical integration of the ray-trace equations on these uniformly sampled grids to investigate the high-frequency part of the wavefield. Most computer software programs designed to study the propagation of seismic energy using the method of ray tracing, however, now use a more efficient approach. Their technique is to decompose the model into layers with the same seismic velocity or the same gradient in seismic velocity. The interfaces separating these layers are represented mathematically as smooth, single-valued functions of depth. Unfortunately, the earth's interior and especially most the areas of interest to exploration geophysicists are not at all smooth. After geologically simple and accessible sedimentary regions have been explored for hydrocarbon resources, interest increases in understanding the propagation of seismic waves in complex geology such as that sketched in Figure 3.1.

Triangles are well suited to represent models of this complexity. Overhanging structures, faulted interfaces and lens-type structures can be easily included into the model. Moreover, such a characterization allows one to store the parameters of the model in such a way, that values on the other side of the edges of the triangle can be determined without searching through the model. This property is especially valuable for efficient ray tracing.

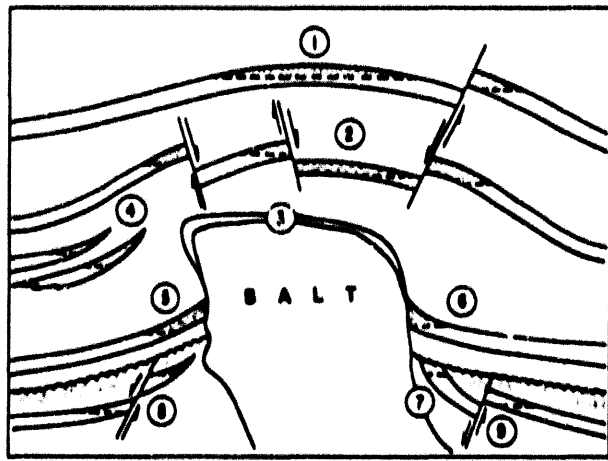


FIG. 3.1. Idealized diapiric salt structure showing common types of hydrocarbon traps (after Tearpock and Bischke, 1990).

3.2 Reflection and Transmission Sequences

Hale (1991) demonstrated how complicated models such as the salt dome in Figure 3.2 can be triangulated for efficient ray tracing. To yield analytic solutions to kinematic and dynamic ray-tracing equations (see Chapter 2), the velocity field in each triangle is constrained to have a constant gradient in slope. The velocity field has to be prescribed by assigning velocity values at the vertices of each triangle or, alternatively, by providing the slope values for an entire geologic block bounded by interfaces. The latter approach has been used to define the velocity field of the salt dome in the left part of Figure 3.2.

The previous version of the modeling code GBmod was designed to generate reflections from only a single selected reflector during any given run of the program. The approach presented here is more dynamic. The generation of multiple raypaths, for example, requires a certain flexibility in the definition of the interfaces. Previously, any given interface could either reflect or transmit seismic energy, but not both; this definition of interfaces did not allow one to trace multiple reflections. As illustrated in Figure 3.3, to obtain selected multiples, a sequence of reflections and transmissions has to be defined at each interface of interest. I have installed this new feature in the ray-tracing code. For each reflector, a *reflecting sequence* can now be defined by the user of this modeling software.

The two different families of multiples in Figure 3.3 have been created by instructions similar to those in other Unix Bourne command shells. To generate the multiple raypath between interface **2** and **3** shown on the left side of the figure, the shell parameter statements are the following:

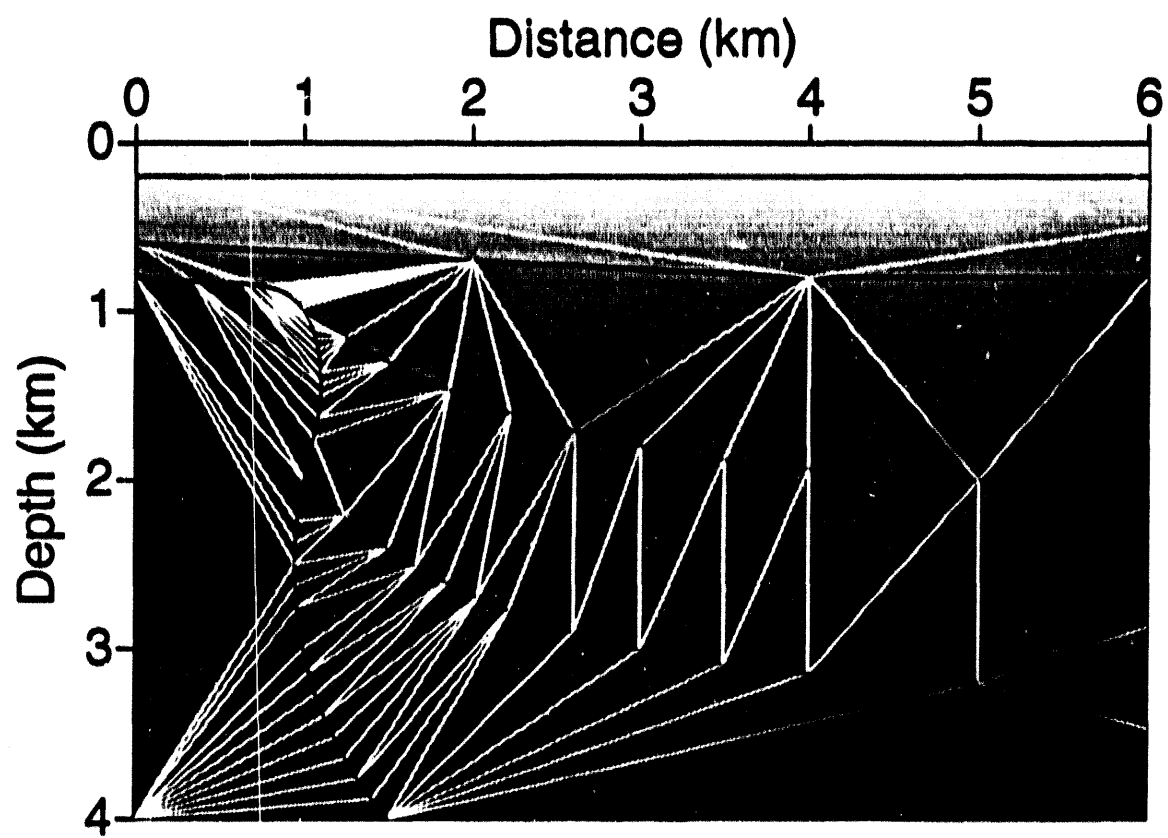


FIG. 3.2. Triangulated model of a salt dome. Note that the model extends to the right of the portion displayed here. The shading denotes the seismic velocity. The specific form and the assigning of the velocity field are discussed in the text.

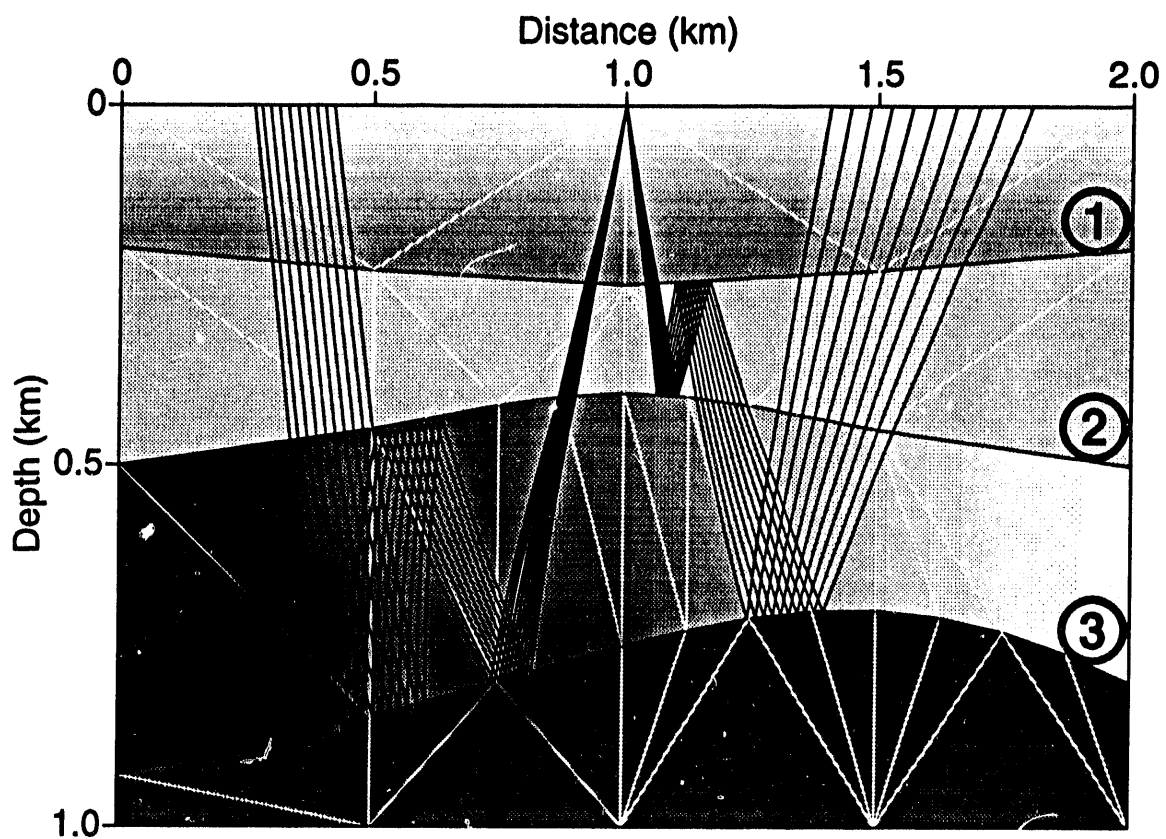


FIG. 3.3. Raypaths for two different families of multiples. Interfaces of interest are labeled. The shading of the different layers indicates that the seismic wave velocity varies with both depth and lateral position.

```

refseq=2,0,1,0 \      # refl./transm. sequence for interface 2
refseq=3,1,1 \      # refl./transm. sequence for interface 3

```

The first number after the equality sign denotes the interface; the following numbers signify the sequence of reflections and transmissions at this interface: "0" denotes transmission, "1" reflection. If no reflection sequence is defined for a reflector, the interface is considered to be only transmitting. In the above case, the first hit on interface 2 will lead to a transmission of the seismic energy, and the second arrival generates a reflection. Finally, the ray propagates towards the surface. For the type of multiple displayed on the right side of Figure 3.3, the following statements are used:

```

refseq=1,0,1,0 \      # refl./transm. sequence for interface 1
refseq=2,1,0,0 \      # refl./transm. sequence for interface 2
refseq=3,1 \      # refl./transm. sequence for interface 3

```

3.3 VSP Modeling Experiment

Recordings from VSP experiments are routinely used to improve the estimation of subsurface properties close to a well. VSP data sets are often more difficult to interpret than are surface data. While common midpoint gathers of surface data bear a certain similarity to actual subsurface structure, the patterns in VSP sections are quite different from the actual configuration in the subsurface. Generation of VSP synthetic data helps to overcome this interpretation problem by providing a tool to help identify events on recorded VSP seismic sections and to check the validity of existing imaging software.

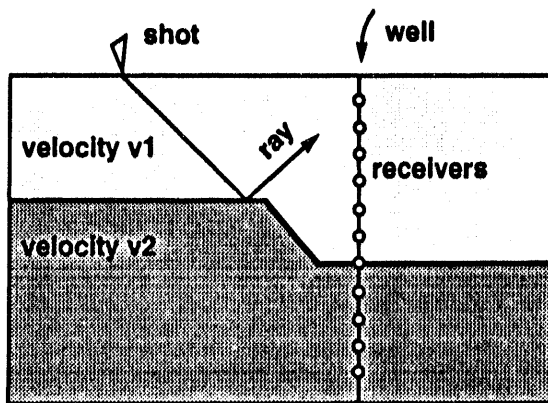


FIG. 3.4. Fault-model VSP experiment with one shot-point. The generated seismic wavefield is recorded by geophones in a well. Figures 3.8 and 3.9 show synthetic data and physical-modeling data for this model.

The software described in this paper can be used to generate data for VSP experiments. Consider the fault model shown in Figure 3.4. This model was used by Jaramillo (1993) of the VSP research group at Colorado School of Mines both to analyze the quality of the generated synthetic and physical model data and to use the modeling software as an interpretation tool for the Yucca Mountain Project. The ray-tracing code provides an additional source of model data.

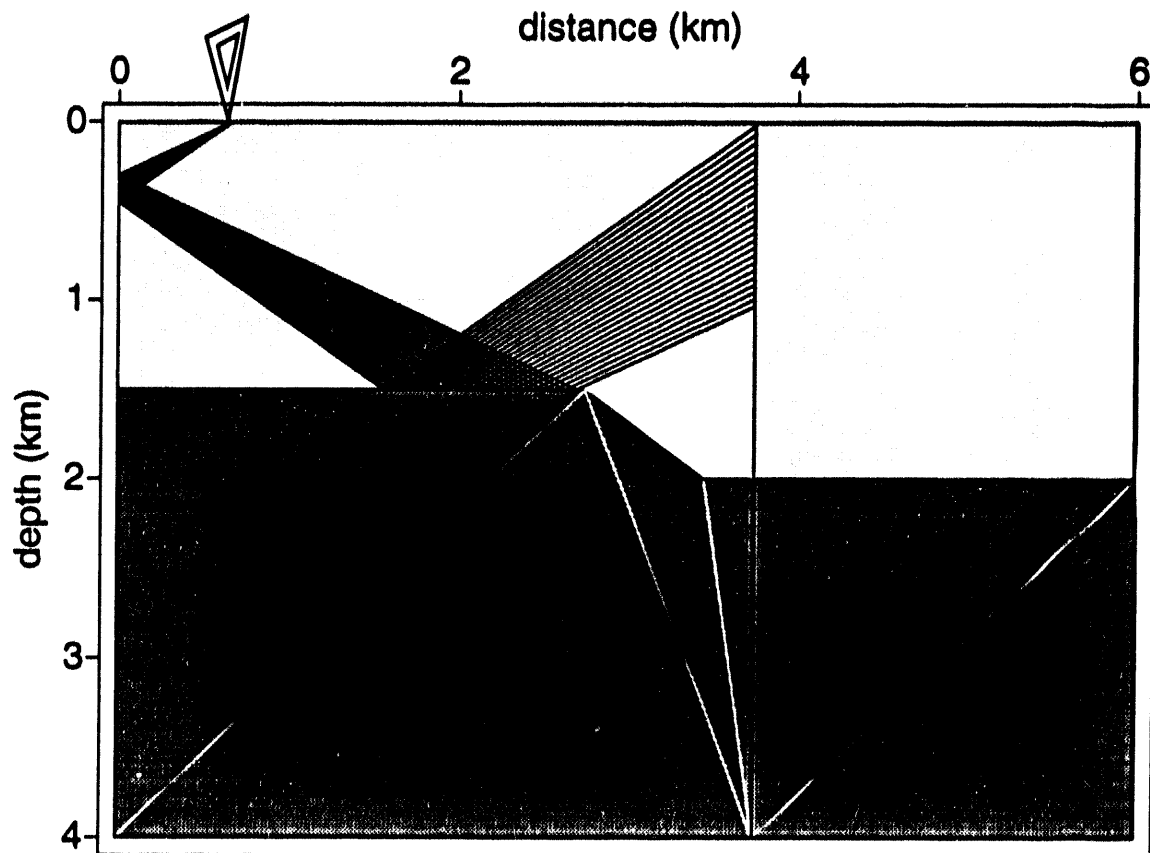
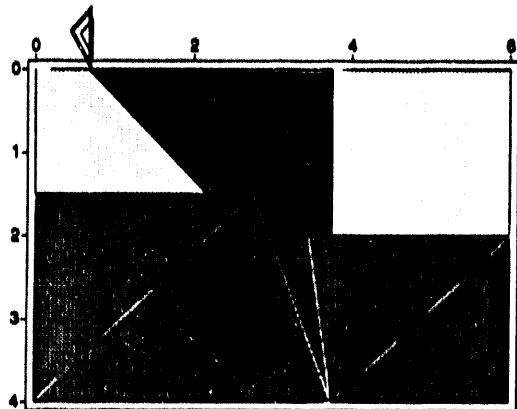


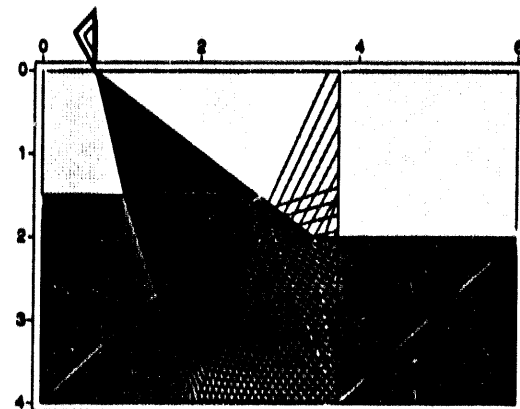
FIG. 3.5. One family of rays generated by the modeling program. The event is recorded by receivers in the vertical borehole. The corresponding reflection in the synthetic seismic section in Figure 3.8 is labeled i.

Figure 3.5 shows one family of rays generated by the modeling software. Two reflections are considered in the ray propagation: the first is at the left boundary of the model, and the second at the hanging wall. The rays finally are recorded by receivers in the borehole.

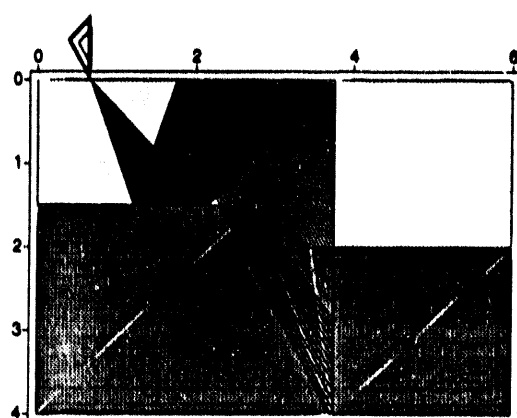
If the left boundary of the model is labeled 1, the faulted interface 2, and the borehole 3, the UNIX command shell for this experiment contains the lines:



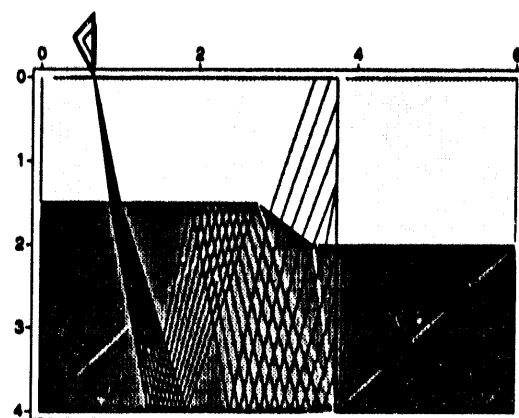
a



b

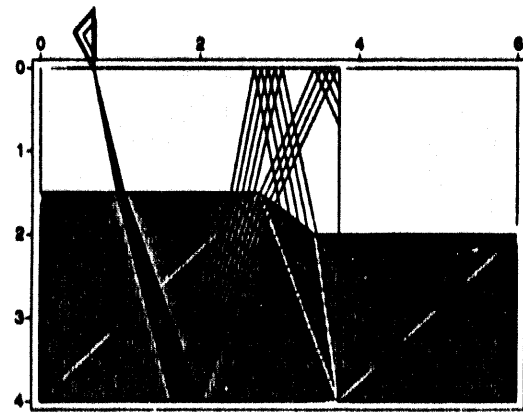


c

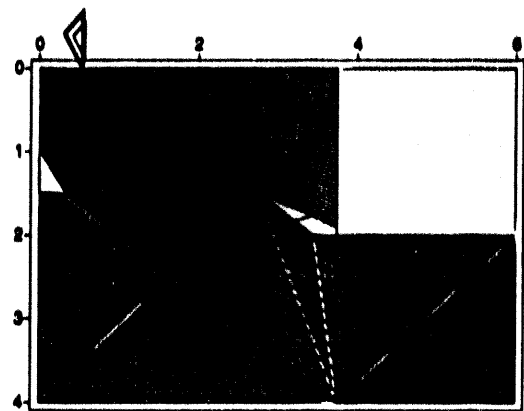


d

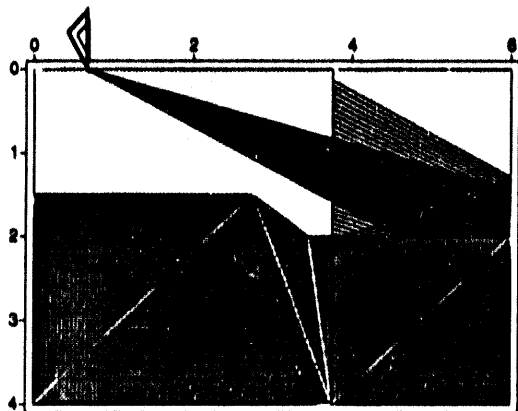
FIG. 3.6. Four different ray types are shown. In example **a**, both direct arrivals and primaries from the foot wall and the hanging wall are present. **b** displays bottom reflections and direct arrivals, **c** surface multiples and **d** bottom multiples. The corresponding seismic events are labeled accordingly in the seismic section shown in Figure 3.8. Note that although the ray density (i.e., increment in takeoff angle) at the source is identical in each figure, the ray coverage at the borehole is different.



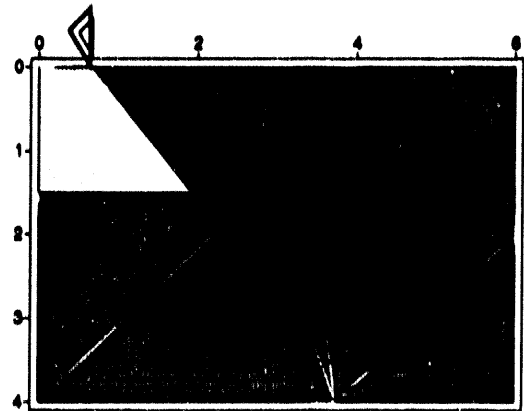
e



f



g



h

FIG. 3.7. The modeling software allows tracing of raypaths that reflect from the sides of the model and that cross the borehole. Rays that are reflected back from the boundary of the model, and pass the receiver line a second time are finally recorded by the geophones in the borehole (see events **g** and **h** in Figure 3.8. As can be seen in **e** and **f**, rays with overcritical incidence are not transmitted.

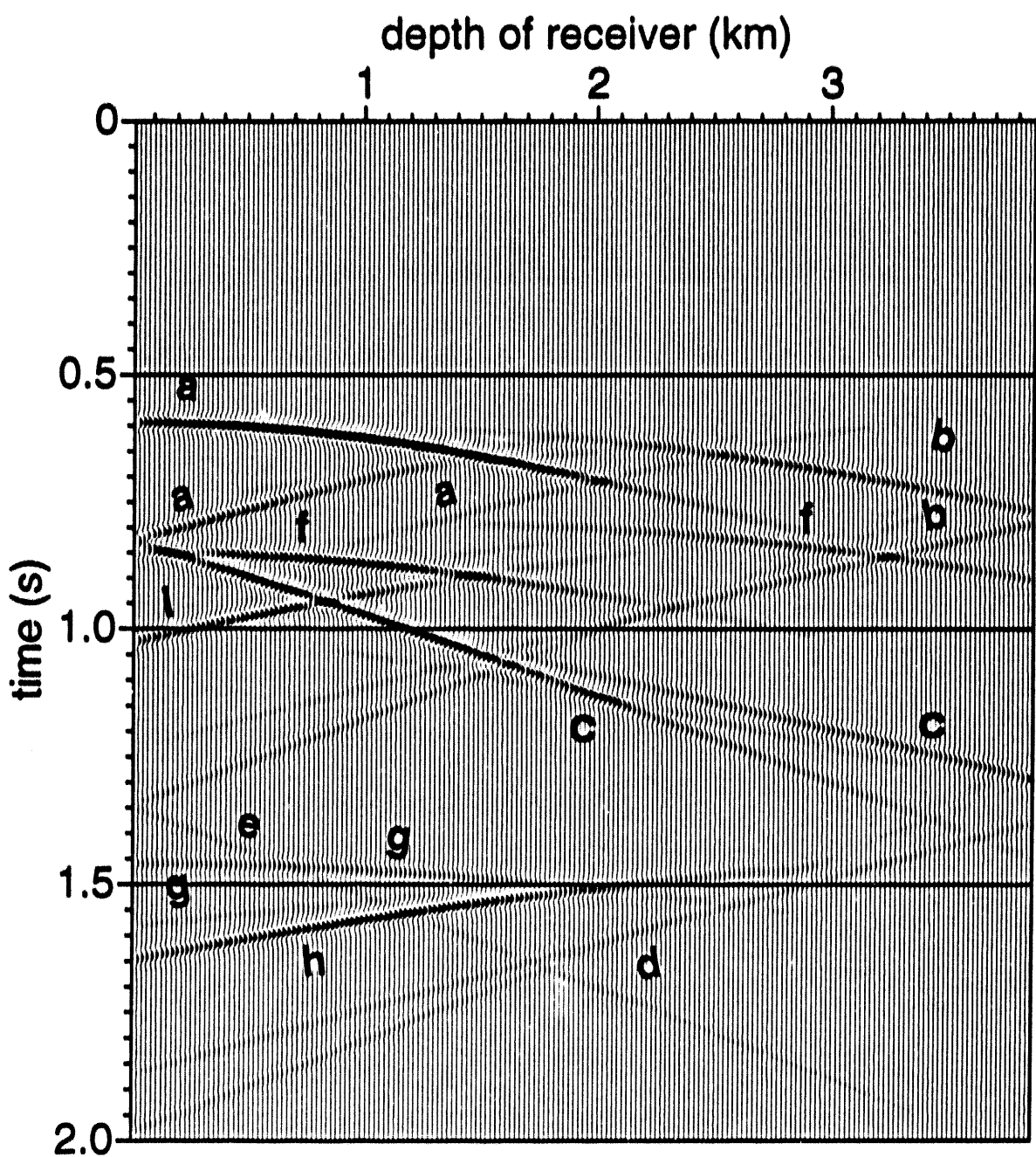


FIG. 3.8. Synthetic data generated by the extended version of Hale's acoustic modeling program. The ray families presented in the previous two figures generate seismic responses that are labeled accordingly here.

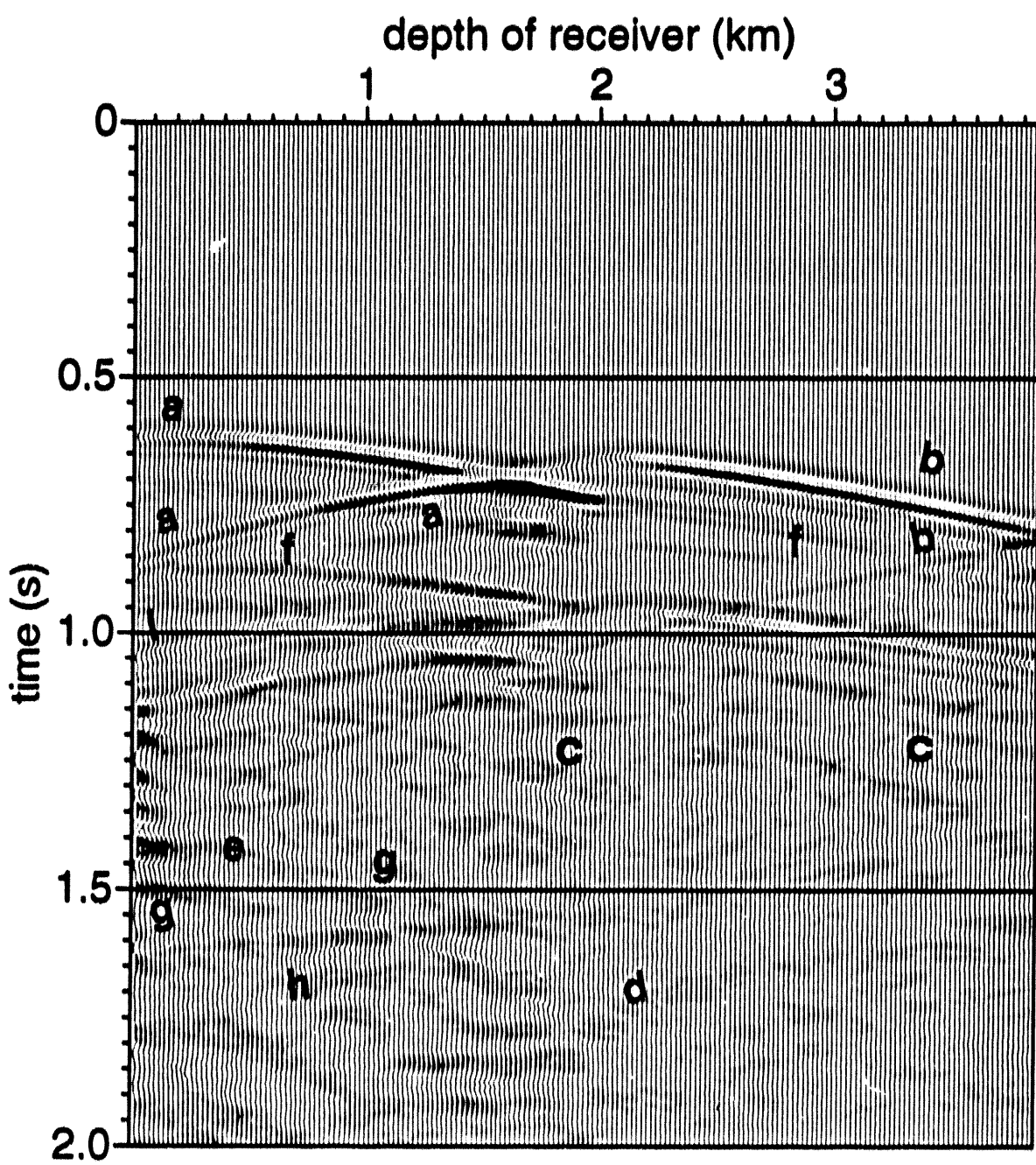


FIG. 3.9. Physical modeling data set after applying a waveform filter to obtain the full P-wave amplitude contribution to the data. Comparison with the synthetic section helps identify most of the dominant coherent events.

```
refseq=1,1 \      # refl./transm. sequence for the left boundary
refseq=2,1 \      # refl./transm. sequence for the fault
refseq=3,-1 \     # refl./transm./stop sequence for the borehole
```

I have previously introduced the designations, "1" for reflection and "0" for transmission; here, I introduce "-1" to denote the stopping of the ray. Thus, the first intersection of the raypath with the borehole terminates the tracing of this ray. Information including the traveltimes, corresponding amplitude, and index of the stopping interface is stored in a file. By default, the rays are stopped at the boundaries of the model. Only rays with the correct stopping index contribute to the events on the seismic section and, optionally, can be displayed. Another feature allows one to select only direct arrivals or only primaries. These new enhancements proved to be helpful in interpreting the physical data gathered in the Yucca Mountain Project.

The synthetic seismic response for the specific event shown in Figure 3.5 is labeled as event **i** in Figure 3.8. This reflection can also be identified in the recorded P-wave physical modeling data (Figure 3.9). In Figures 3.6 and 3.7, a series of ray families is displayed for the same geometry. The letter labels on the models in Figures 3.6 and 3.7 correspond to the events in Figure 3.8. In this form, one can conveniently compare the synthetic section with the physical modeling data to aid in identifying individual events.

The modeling software now allows tracing of all rays of interest. It is possible to specify reflections from the vertical and horizontal boundaries of the model, features that are unavoidably recorded in physical modeling experiments; multiples can be conveniently defined; and rays may also be traced across the borehole before they encounter the receiver line a second time and are recorded (see events **g** and **h**).

Differences in Figures 3.8 and 3.9 can be attributed to a number of factors. Among them is the fact that the ray-trace code presently generates only acoustic events, whereas the physical model is 2-D elastic. For this VSP experiment, the computer run time, including the automated triangulation, the tracing of nine different ray modes, and the generation of the synthetic seismic sections took 23 seconds of CPU time on an IBM RISC System/6000 Model 520 workstation.

Chapter 4

APPLICATION OF DYNAMIC RAY TRACING: RAY DATA AND FRESNEL VOLUMES

In this chapter, the theory introduced in Chapter 2 will be applied to the dynamic ray-tracing modeling software. The media considered are two-dimensional or two-and-one-half-dimensional. Starting with elastic wave propagation, I finally reduce the complexity of modeling by considering only acoustic media. The main differences between elastic and acoustic wave propagation are, however, discussed. The dynamic ray tracing data can be applied to both the acoustic and the elastic case.

4.1 Phase-front Curvature and Paraxial traveltimes

The leading-order solution of the eikonal equation in ray-centered coordinates (2.17) can be used to compute additional quantities along the rays. Equation (2.22) shows that the phase-front curvature matrix \mathbf{M} can be evaluated by $\mathbf{M} = \mathbf{P}\mathbf{Q}^{-1}$, with \mathbf{Q} and \mathbf{P} determined by

$$\begin{pmatrix} \mathbf{Q}(\sigma) \\ \mathbf{P}(\sigma) \end{pmatrix} = \Pi(\sigma_0, \sigma) \cdot \begin{pmatrix} \mathbf{Q}(\sigma_0) \\ \mathbf{P}(\sigma_0) \end{pmatrix}.$$

In two-dimensional computations, the quantities M , p and q are the scalar equivalents of matrices \mathbf{M} , \mathbf{P} and \mathbf{Q} .

Knowledge of the phase-front curvature \mathbf{M} is exploited for various applications. For example, it can be used to compute the traveltime in the vicinity of the ray. This is of practical importance for the modeling software because, in general, rays do not emerge exactly at the position of the receivers.

Consider Figure (4.1) showing receiver position R and the endpoint of a ray E . Δs denotes the difference in arclength, and n is the perpendicular distance from the receiver to the ray. Assuming the dynamic ray-tracing data to be known at point E , the *paraxial travelttime* $\tau(R, E)$ can be approximated by:

$$\begin{aligned} \tau(R, E) &\approx \tau(E) + \frac{\partial \tau}{\partial s} \Delta s + \frac{1}{2} \frac{\partial^2 \tau}{\partial s^2} (\Delta s)^2 + \frac{1}{2} n^2 M(E) \\ &\approx \tau(E) + \frac{1}{v(E)} \Delta s - \frac{1}{2} \frac{1}{v^2(E)} \frac{\partial v(E)}{\partial s} (\Delta s)^2 + \frac{1}{2} n^2 M(E). \end{aligned} \quad (4.1)$$

The Taylor expansion (4.1) involves the gradient of velocity in ray direction. While this term is often neglected in the extrapolation of traveltimes in smooth media, it is important if one considers more complex models. In these media, rays often emerge at the surface with angles close to horizontal and yield significant values of Δs . As discussed in

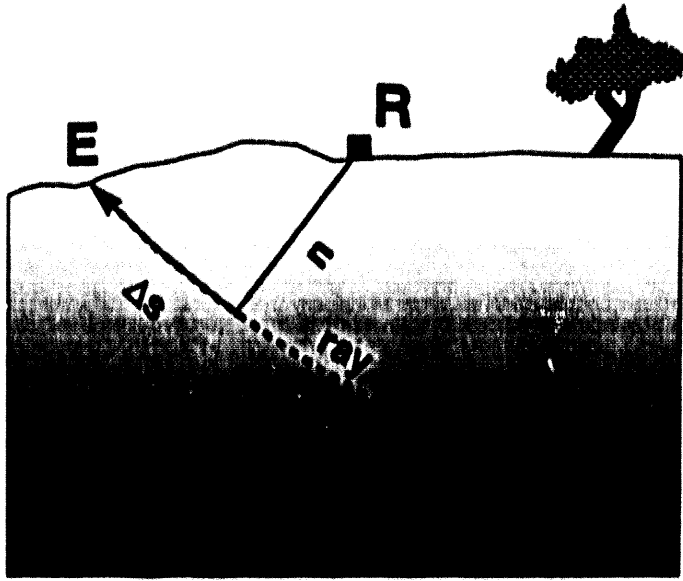


FIG. 4.1. The approximate traveltime at any point S in the vicinity of the ray can be evaluated by using the dynamic ray tracing data at point O_S .

Chapter 5, the same is true for the Gaussian beam method, because this method requires traveltime-extrapolation far away from the ray if strong velocity variations are present. I implemented this term in the program GBmod. However, despite these modifications, note that this approach is valid only for a smooth velocity field in the vicinity of ray ends and receivers. Strong velocity gradients or jumps in velocity lead to inaccurate paraxial traveltime data.

4.2 Ray Amplitudes

In Chapter 2, I showed that, to first order accuracy, high-frequency pressure waves (P-waves) and shear waves (S-waves) propagate independently through smooth media. In other words, the amplitude vector $U_i^{(0)} (= U_i)$ in equation (2.3) can be represented in the form:

$$U_i = U_1^{(q)} \cdot \hat{e}_1 + U_2^{(q)} \cdot \hat{e}_2 + U_3^{(q)} \cdot \hat{t},$$

where \hat{e}_1 , \hat{e}_2 and \hat{t} span the ray-centered coordinate system. Recall that this system, together with the kinematic and dynamic-ray tracing equations, can be derived from equation (2.4). Several textbooks (e.g., Aki and Richards, 1980; Červený, 1985a) show explicitly how equation (2.5) can be used to solve for the components $U_1^{(q)}$, $U_2^{(q)}$ and $U_3^{(q)}$. This derivation is tedious and time-consuming and will not be repeated here. The

solution obtained is of the following form:

$$U_i^{(q)}(\sigma) = \sqrt{\frac{v(\sigma_0) \rho(\sigma_0) J(\sigma_0)}{v(\sigma) \rho(\sigma) J(\sigma)}} U^{(q)}(\sigma_0). \quad (4.2)$$

Here, v , ρ and J denote velocity, density and the ray Jacobian, respectively. Velocity and the ray Jacobian are different for P-waves and S-waves. $U^{(q)}(\sigma_0)$ is a quantity influenced by the source radiation pattern. The vectorial amplitude for P-waves is

$$U_i = U_3^{(q)} \cdot \hat{t}; \quad v = v_{\text{P-wave}}, \quad J = J_{\text{P-wave}}.$$

The S-wave can be represented by

$$U_i = U_1^{(q)} \cdot \hat{e}_1 + U_2^{(q)} \cdot \hat{e}_2; \quad v = v_{\text{S-wave}}, \quad J = J_{\text{S-wave}}.$$

In the ray-centered coordinate system $(\hat{e}_1, \hat{e}_2, \hat{t})$, the S-waves have two decoupled components perpendicular to the ray.

In acoustic media of constant density, the solution of the transport equation has to be modified, because it is pressure (or the potential of u_i) that is observed.

$$\text{pressure amplitude} = U_{\text{acoustic}} = \sqrt{\frac{v(\sigma)}{v(\sigma_0)}} \sqrt{\frac{J(\sigma_0)}{J(\sigma)}} \cdot U(\sigma_0).$$

Dynamic ray tracing is well suited to handle the elastic, three-dimensional case. In fact, most authors deal exclusively with the elastic case. Computationally, the evaluation of \hat{e}_1 and \hat{e}_2 and the introduction of both P-waves and S-wave velocities are the main considerations required in extending the acoustic case. However, to reduce the complexity of the following derivations and test the applicability of the method for structures of higher complexity, we restrict ourselves to acoustic wavefields.

In acoustic media, the first term of the ray series yields

$$u(\sigma) = \sqrt{\frac{v(\sigma)}{v(\sigma_0)}} \sqrt{\frac{J(\sigma_0)}{J(\sigma)}} \cdot U(\sigma_0) \cdot \exp(-i\omega(t - \tau(\sigma))).$$

The ray Jacobian J and its relation to the results of the dynamic ray tracing are derived in Appendix B. Note that the choice of coordinate systems differs from those in the literature (for computational reasons, σ and not the arclength s is used as the running parameter along the ray). Considering the result derived in the appendix, the first term in the ray series yields

$$u(\sigma) = \sqrt{\frac{v(\sigma)}{v(\sigma_0)}} \sqrt{\frac{\det \mathbf{Q}(\sigma_0)}{\det \mathbf{Q}(\sigma)}} \cdot U(\sigma_0) \cdot \exp(-i\omega(t - \tau(\sigma))). \quad (4.3)$$

Hence, if we know $v(\sigma_0)$, the velocity at the source, the velocity at the ray end $v(\sigma)$ and

the dynamic ray tracing results \mathbf{Q} and \mathbf{P} , we can approximately solve the wave equation along a ray and in its paraxial vicinity. The corresponding equation for two-dimensional media involves the scalar quantity q evaluated from equation (2.26) instead of the matrix \mathbf{Q} .

$$u(\sigma) = \sqrt{\frac{v(\sigma)}{v(\sigma_0)}} \sqrt{\frac{q(\sigma_0)}{q(\sigma)}} \cdot U(\sigma_0) \cdot \exp(-i\omega(t - \tau(\sigma))). \quad (4.4)$$

4.3 Attenuation

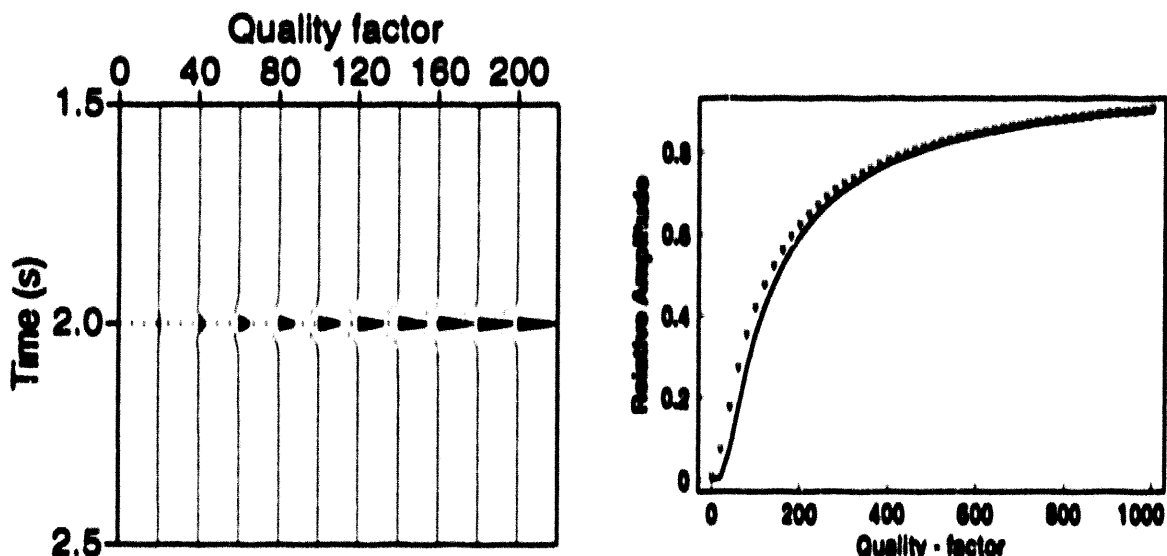


FIG. 4.2. Synthetic seismograms displayed as a function of quality factor Q . The receiver is situated in a homogeneous medium, 5 km from a point source. Velocity of the medium is 2.5 km/s. Only noncausal attenuation is evaluated. The solid line in the right diagram represents analytically computed pressure amplitudes at peak frequency; the triangles denote modeled peak-frequency amplitudes. The amplitudes are scaled relative to the amplitude value obtained in an non-absorbing medium.

Recorded seismic data are influenced by anelastic properties of the subsurface. I added an option that allows one to assign a constant attenuation value to each geologic block bounded by interfaces. The implementation of noncausal absorption (i.e., only the reduction of the amplitude is considered, phase changes due to attenuation are neglected) into the program GBmod is made efficient by introducing a complex velocity using the *Debye approximation* (Müller, 1983).

$$\frac{1}{v} \pm \frac{1}{v_{real}} \cdot \left(1 + \frac{i}{2Q}\right),$$

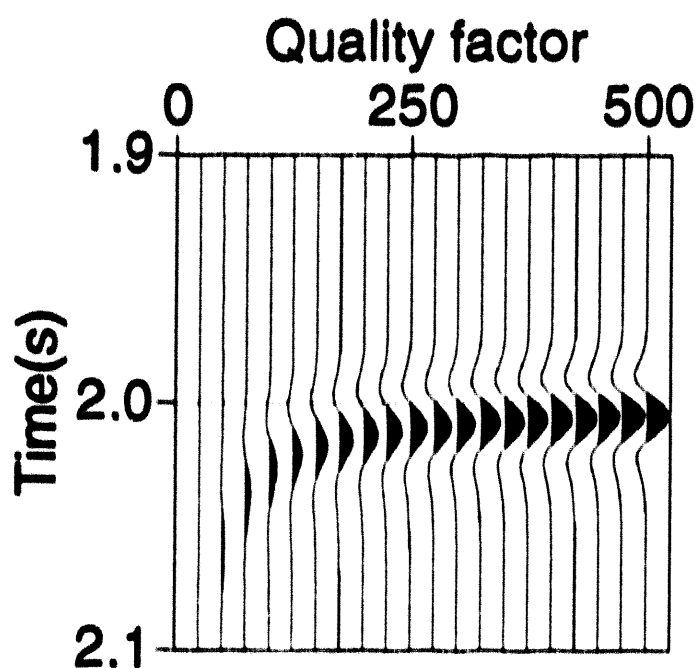


FIG. 4.3. Synthetic seismograms displayed as a function of quality factor Q . The receiver is situated in a homogeneous medium, 5 km from a point source. A zero-phase Ricker wavelet is propagated from the source to the receivers. Velocity of the medium is 2.5 km/s. Causal absorption is included and disturbs the Ricker wavelet. For low values of Q , one observes a significant time-delay and wave-form distortion.

where v_{real} is the specified real-valued seismic velocity, and Q is the quality factor for dissipative wave propagation. For ω denoting radial frequency and s , the monotonically increasing arclength along the ray, the amplitude decay A_{decay} due to attenuation is given by

$$A_{decay} = \exp\left(-\omega \int_{s_0}^s \frac{1}{2Qv_{real}} ds\right) = \exp(-\omega t^*) .$$

For a constant Q in each triangle, the *global absorption factor*

$$t^* = \int_{s_0}^s \frac{1}{2Qv_{real}} ds = \sum_{i=1}^{i=N} \frac{t_i}{2Q_i}$$

can be obtained as a simple by-product of the ray tracing. Here, N is the number of triangles traversed and Q_i and t_i are the quality factor and the travelttime within the i th triangle. Figure 4.2 is a display of the seismic response of a homogeneous, absorbing medium with $v_{real} = 2.5$ km/s. The receiver is situated 5 km from the source. Each trace corresponds to a different value of quality factor Q . The right diagram shows the dominant-frequency amplitude versus Q . The solid line represents the analytically computed values, the triangle symbols denote results computed by the Gaussian beam modeling. The values are normalized by setting the amplitude for the perfectly elastic medium to unity. Note that the accuracy increases with decreasing absorption in the medium. However, even for small values of Q , the comparison is satisfactory.

Multiplication of the amplitudes evaluated for non-absorbing media by the amplitude decay factor A_{decay} in the frequency domain yields noncausal results. I implemented a phase-correction proposed by Červený (1987) to simulate causal absorption (see Figure 4.3). For decreasing Q , one recognizes a similar decay in amplitude as in the noncausal case, but also a delay of the causal signal towards larger travelttime. A more detailed examination shows that the signals broaden and become slightly asymmetric. The efficiency of the noncausal treatment in dissipative models is essentially the same as in perfectly elastic models. The computational cost of including causal attenuation effects, however, is significantly higher; therefore, in the Gaussian beam modeling program GBmod, the causal feature is optional.

4.4 Two-And-One-Half-Dimensional Spreading

In the program, I included a computationally simple procedure to correct for geometrical spreading for a point source in the medium. Previously, the modeling yielded amplitudes for a line source with cylindrical-wave expansion. I used the three-dimensional dynamic ray-tracing equation to derive the necessary amplitude correction (see Chapter 2). Consider variations of the properties of the medium to be restricted to the (x_1, x_3) -plane, with no variations in the x_2 -direction allowed. As derived in equation (4.3), the pressure amplitude is anti-proportional to the square-root of the determinant of matrix

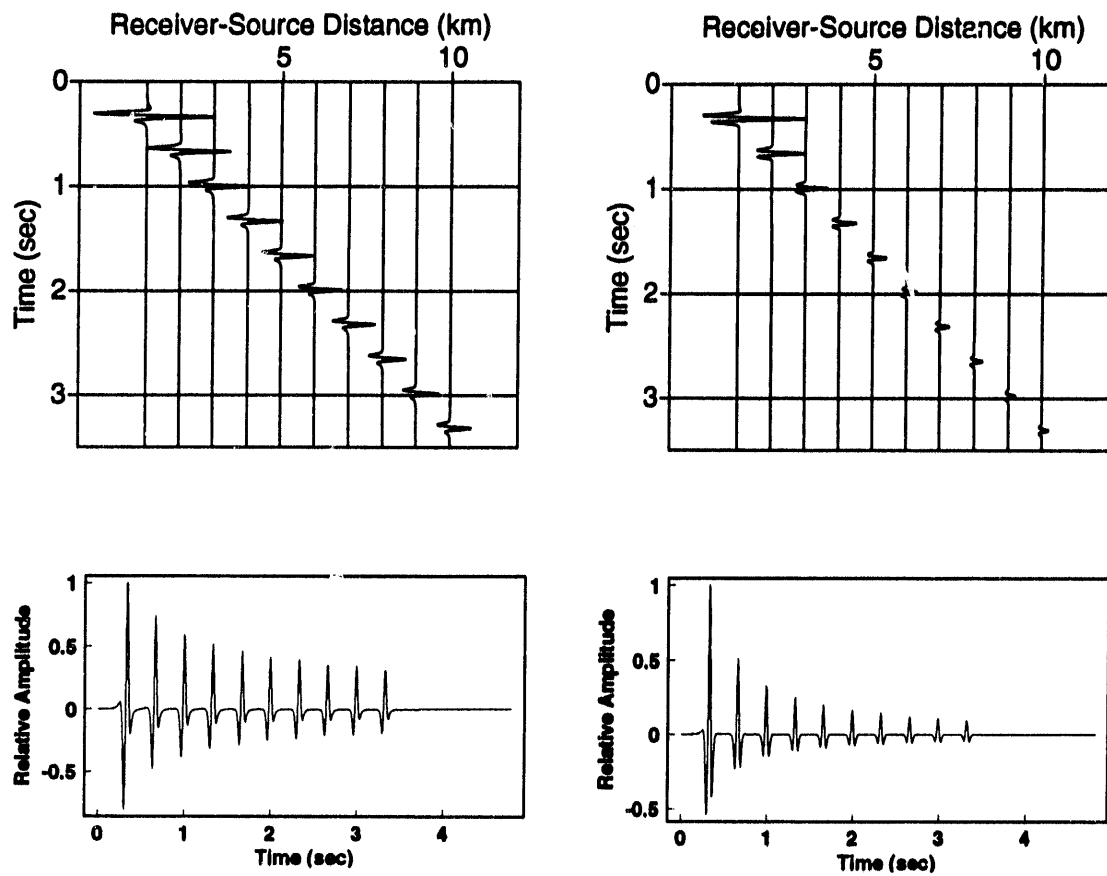


FIG. 4.4. Seismic sections generated by Gaussian beam modeling in homogeneous media. The right side simulates the energy spreading due to a point source; the left time section shows the response due to a line source. Below, the seismic traces of each section are added to help see the difference in amplitude decay.

Q. In 2.5-D media, this expression reduces to

$$\sqrt{Q} = \sqrt{Q_{11} Q_{22}} .$$

Using equation (2.29), the factor that multiplies the original two-dimensional solution is proportional to

$$\left(\int_{s_0}^s v \, ds \right)^{-\frac{1}{2}} = (\sigma - \sigma_0)^{-\frac{1}{2}},$$

where σ is a running parameter of units [length²/time], and s is the arclength increasing from s_0 to s along the ray. Figure 4.4 emphasizes the difference in amplitude decay for homogeneous 2-D and 2.5-D media. To help see the spreading behavior, the 10 traces of each seismic section are summed and displayed in the lower part of the figure. The amplitude decay is proportional to $r^{-\frac{1}{2}}$ for the line source and r^{-1} for the point source, where r is the distance traveled.

4.5 Fresnel-Volume Ray Tracing

The term *Fresnel-volume* was introduced by Kravtsov and Orlov (1990) to generalize the concept of Fresnel-zones. These authors suggested that rays be considered as physical objects rather than volumeless trajectories. Stated differently, all points within a region in the vicinity of the ray, the Fresnel-volume, influence the wave propagation associated with this ray. As illustrated in Figure 4.5, a point F belongs to the Fresnel-volume of the

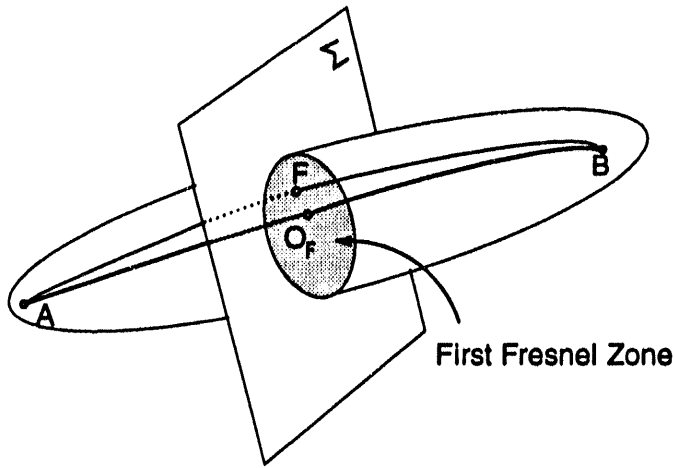


FIG. 4.5. The Fresnel-volume for a ray from A to B. The point O_F marks the intersection of the ray with the plane Σ . Points such as F influence the wavefield along the ray if the *Fresnel condition* (4.5) is satisfied.

ray from A to B if the *Fresnel condition* (4.5) is satisfied (see also Červený and Soares [1992]), that is

$$|\tau(F, A) + \tau(F, B) - \tau(B, A)| \leq \frac{1}{2}T. \quad (4.5)$$

Here, T denotes the dominant period of the signal, and $\tau(F, A)$, $\tau(F, B)$ and $\tau(B, A)$ are the traveltimes from F to A , F to B and B to A , respectively. Fresnel-volumes depend on the velocity field close to the ray as well as on the dominant frequency of the signal.

I used recent work by Červený and Soares (1992) to supplement the dynamic ray-tracing routine in the modeling code GBmod with an option to compute the two-dimensional paraxial approximation of the Fresnel-volume. This may be performed efficiently and accurately by using the elements of the ray-propagator matrix, which are evaluated in the dynamic ray tracing. Fresnel-volume ray tracing (or *physical ray trac-*

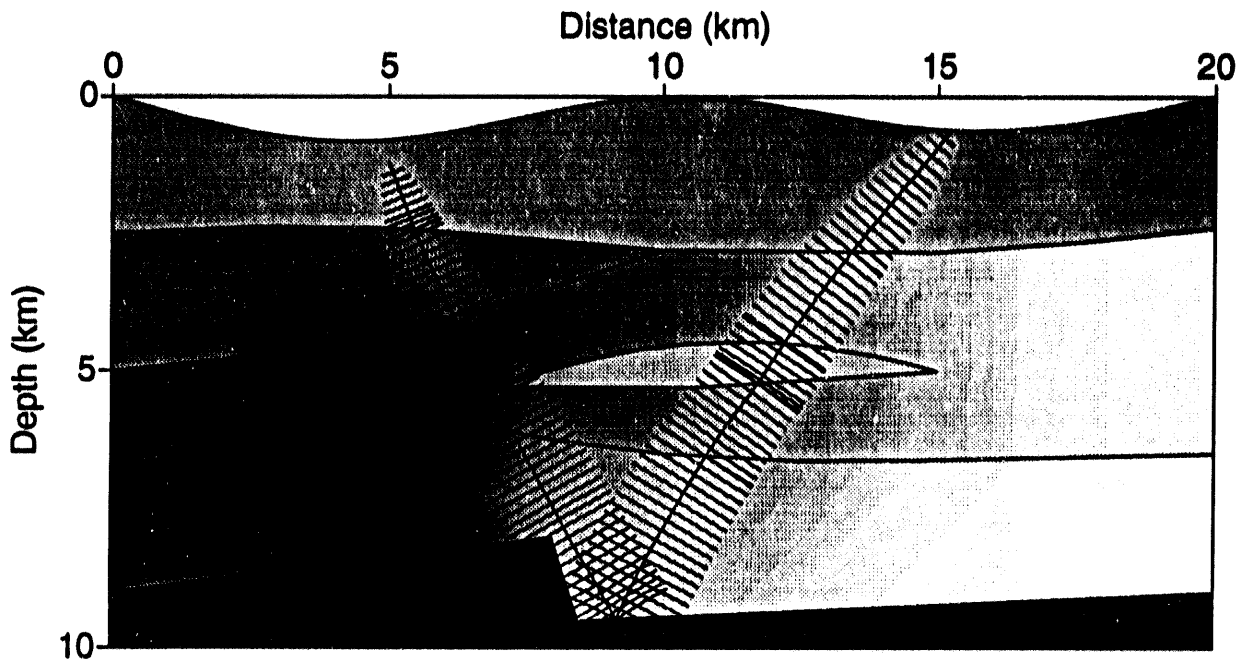


FIG. 4.6. The Fresnel-volume for a ray traveling through an inhomogeneous medium. A signal frequency of 5 Hz is considered. Intersections of the Fresnel-volume with the edges of the lens and the fault indicate a violation of the ray-theoretical assumptions.

ing) offers several applications for the field of exploration geophysics. For example, study of the resolution of the seismic method can be extended to complicated media, and the validity conditions of ray methods can be stated explicitly in terms of the radius of the Fresnel-zone at any point along a specified raypath (see Kravtsov and Orlov, 1990). In Figure 4.6, the plot of the Fresnel-volume (actually, Fresnel area, for these 2-D models) for a signal frequency of 5 Hz indicates that the ray-theoretical assumptions are violated

because the edges of the fault and the velocity lens intersect the Fresnel-volume. The wavefield along the ray is, in this sense, obstructed. The wavefield recorded at the receiver is influenced by the zone covered by this Fresnel-volume and not only by the line traced by the classical ray.

Chapter 5

THE GAUSSIAN BEAM METHOD

5.1 Why Do We Use the Gaussian Beam Method?

So far, the majority of issues addressed in this thesis involved the tracing of rays and the computation of helpful information such as out-of-plane spreading or Fresnel-volumes. In the modeling software GBmod, these quantities and the results of kinematic and dynamic ray tracing are evaluated at the ray ends and stored in a file. Several methods have been proposed to use these data to generate synthetic seismograms, among them are the *paraxial method* (e.g. Beydoun and Keho, 1987) and the Gaussian beam method (e.g., Červený, et al, 1982).

The Gaussian beam method (GBM) was first introduced to the field of geophysics by Popov (1982) and Červený et al. (1982). These authors proposed to expand a source wavefield into Gaussian beams, which are individually computed from the source to their endpoints. The seismic wavefield at each receiver is then evaluated by integrating over all beams in the vicinity of the receiver. The GBM therefore considers not only the information provided by the nearest beam, but the information of all beams in the neighborhood. This procedure has several advantages. First, rays (which are the support of the beams) are no longer required to stop at the exact position of each receiver; thus time-consuming two-point ray tracing can be avoided. Second, the GBM yields stable results in regions of the wavefield where the standard ray theory fails (e.g., caustics, shadow zones and critical distance). Third, unlike seismograms computed by conventional ray tracing techniques, the GBM synthetic data are less influenced by minor details in the model representation. These advantages are discussed and illustrated for example in Červený, (1985b), where more references can be found. This chapter gives an introduction to the theory of Gaussian beams. A good knowledge of the theory is necessary to best understand the limitations of the method when dealing with complex subsurface structures.

5.2 Gaussian Beam Theory

Two main derivations of the GBM are found in the literature. The first approach, the so-called parabolic wave equation method, uses the reduction of the wave equation to a parabolic equation for each individual wave type. This procedure is described in detail in Červený and Pšenčík (1983) and has the advantage of explicitly deriving the Gaussian beams as the high-frequency asymptotic solutions of the wave equation close to rays.

Here, I use a different way to introduce the GBM. As shown in Červený (1985a), the dynamic ray-tracing procedure introduced in Chapter 2 can be generalized by allowing the eikonal function $\tau(x_i)$ to be complex valued. More strictly, the traveltimes is real

valued at the rays and complex valued outside the rays. Under certain conditions, which will be introduced below, the high-frequency solution of the elastodynamic equation with a complex-valued phase function is called a *Gaussian beam*. In other words, the beam can be considered as a paraxial ray approximation with a complex valued traveltime. Recall that, for two-dimensional media, the traveltime in the vicinity of a ray can be expressed in the form

$$\tau(\mathbf{S}) \approx \tau(\mathbf{O}_S) + \frac{1}{2} M n^2, \quad (5.1)$$

where M is the phase-front curvature evaluated along the ray, \mathbf{O}_S is the orthogonal projection of \mathbf{S} on the ray and n is the perpendicular distance to the ray. In classical dynamic ray tracing (paraxial ray tracing), M is real valued, whereas in the Gaussian beam method, M is complex.

$$M = \operatorname{Re}(M) + i \operatorname{Im}(M).$$

For $\operatorname{Im}(M) = 0$, the Gaussian beam solution reduces to the paraxial ray solution. As shown in Chapter 2, the seismic ray-theoretical pressure at a receiver \mathbf{S} in a two-dimensional acoustic medium can be described by:

$$u(\mathbf{S}) = \sqrt{\frac{v}{v_0}} \sqrt{\frac{q_0}{q}} U_0 e^{-i\omega(t-\tau(\mathbf{S}))}. \quad (5.2)$$

q and q_0 are dynamic ray-tracing quantities corresponding to the matrix \mathbf{Q} in the three-dimensional case. After expanding the traveltime τ according to equation (5.1), the exponential can be written in the form

$$\exp \left[-i\omega \left(t - \tau(\mathbf{O}_S) - \frac{1}{2} M(\mathbf{O}_S) \cdot n^2 \right) \right].$$

Allowing M to be complex yields

$$\exp \left[-i\omega \left(t - \tau(\mathbf{O}_S) - \frac{1}{2} \operatorname{Re}(M) \cdot n^2 \right) \right] \cdot \exp \left[-\frac{\omega}{2} \operatorname{Im}(M) \cdot n^2 \right].$$

Introducing the frequency-dependent beam width

$$L(\mathbf{O}_S, \omega) = \sqrt{\frac{2}{\omega} \cdot (\operatorname{Im}(M(\mathbf{O}_S))^{-1}},$$

i.e., the distance from the central ray at which the amplitude of the Gaussian beam is $\frac{1}{e}$ -times the amplitude on the central ray, and the curvature of the wavefront

$$K(\mathbf{O}_S) = -v \operatorname{Re}(M),$$

equation (5.2) takes the form

$$u(S) = \sqrt{\frac{v}{v_0}} \sqrt{\frac{q_0}{q}} U_0 \exp \left[-i\omega \left(t - \tau(O_S) + \frac{K(O_S)}{2v} n^2 \right) \right] \cdot \exp \left[-\frac{n^2}{L^2} \right]. \quad (5.3)$$

A sketch of the amplitude profile perpendicular to the central ray is shown in Figure 5.1.

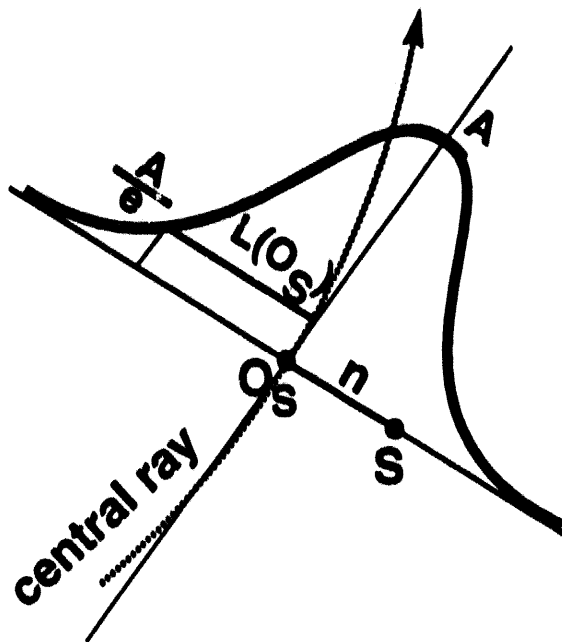


FIG. 5.1. Amplitude profile of a Gaussian beam

Solutions of the form (5.3) are called Gaussian beams if the following two assumptions are satisfied along the ray:

- $\text{Im}(M) > 0$
- $q \neq 0$.

The first assumption guarantees the concentration of the solution close to the central ray. Second, quantity q describing the geometrical spreading must be nonzero and finite along the ray; thus Gaussian beams, unlike the conventional ray solutions, are nonsingular even at caustics of the wavefield.

The fundamental matrix

$$\Pi(\sigma_0, \sigma) = \begin{pmatrix} q_1(\sigma) & q_2(\sigma) \\ p_1(\sigma) & p_2(\sigma) \end{pmatrix},$$

i.e., the set of linearly independent, real dynamic ray-tracing solutions for the two-dimensional case (equations [2.26]), with

$$\Pi(\sigma_0, \sigma_0) = \begin{pmatrix} 1 & 0 \\ 0 & 1 \end{pmatrix},$$

can be directly applied to solve for the complex quantity M . Analogous to the three-dimensional case studied in Chapter 2, any solution $p(\sigma)$ and $q(\sigma)$ can be evaluated as a linear combination of the dynamic ray tracing results :

$$\begin{aligned} p(\sigma) &= z_1 p_1(\sigma) + z_2 p_2(\sigma), \\ q(\sigma) &= z_1 q_1(\sigma) + z_2 q_2(\sigma), \end{aligned}$$

where, in general, z_1 and z_2 are complex valued constants. Introducing the complex valued beam parameter $\epsilon = z_1/z_2$ yields the following equation for M :

$$M = p/q = \frac{\epsilon p_1 + p_2}{\epsilon q_1 + q_2}.$$

The beam width L and the curvature K can now be expressed in terms of the complex parameter $\epsilon = \epsilon_1 + i\epsilon_2$:

$$\begin{aligned} L &= \sqrt{-\frac{2}{\omega} \cdot \frac{(\epsilon_1 q_1 + q_2)^2 + (\epsilon_2 q_1)^2}{\epsilon_2}}; \\ K &= -v \frac{(\epsilon_1 p_1 + p_2)(\epsilon_1 q_1 + q_2) + \epsilon_2^2 p_1 q_1}{(\epsilon_1 q_1 + q_2)^2 + (\epsilon_2 q_1)^2}. \end{aligned} \quad (5.4)$$

Recall that $q_1(\sigma_0) = 1$, $p_1(\sigma_0) = 0$, $q_2(\sigma_0) = 0$, $p_2(\sigma_0) = 1$; so that the following beam width and curvature are found at the source:

$$L = \sqrt{-\frac{2}{\omega} \cdot \frac{\epsilon_1^2 + \epsilon_2^2}{\epsilon_2}}; \quad (5.5)$$

$$K = -v \frac{\epsilon_1}{\epsilon_1^2 + \epsilon_2^2}. \quad (5.6)$$

In summary, the GBM can be seen as one specific application of the dynamic ray-tracing results. For each beam, the dynamic ray-tracing data q_1 , q_2 , p_1 and p_2 are weighted by a complex parameter ϵ . The choice of ϵ determines the frequency-dependent width of the beam as well as the phase-front curvature.

5.3 Difficulties with the Gaussian Beam Approach

Several methods have been proposed to use kinematic and dynamic ray tracing data to generate synthetic seismograms, among them are the paraxial method and the Gaussian beam method. Both of these methods share the advantage that time-consuming

two-point ray tracing is not required. In the paraxial method, the seismic response at a receiver is calculated by extrapolating the information provided by the nearest ray. The GBM uses a weighted sum of information of all rays in the vicinity of the receiver. Although this procedure is computationally more difficult and less efficient, it offers the advantage that the results are regular even in regions, where the conventional ray methods fail (e.g., caustics or shadow zones). These situations are extensively discussed in the literature (e.g. Weber, 1988; Kästner and Fritsche, 1988; Müller, 1984), and several examples of computations of GBM results are shown. None of these references, however, provides examples of using the GBM in models of significant complexity, such as in Figure 5.2, nor do they consider reflections from more than one target. To improve our understanding of the difficulties that influence the Gaussian beam solutions for models with strong inhomogeneities, a quick review of the Gaussian beam summation approach is necessary.

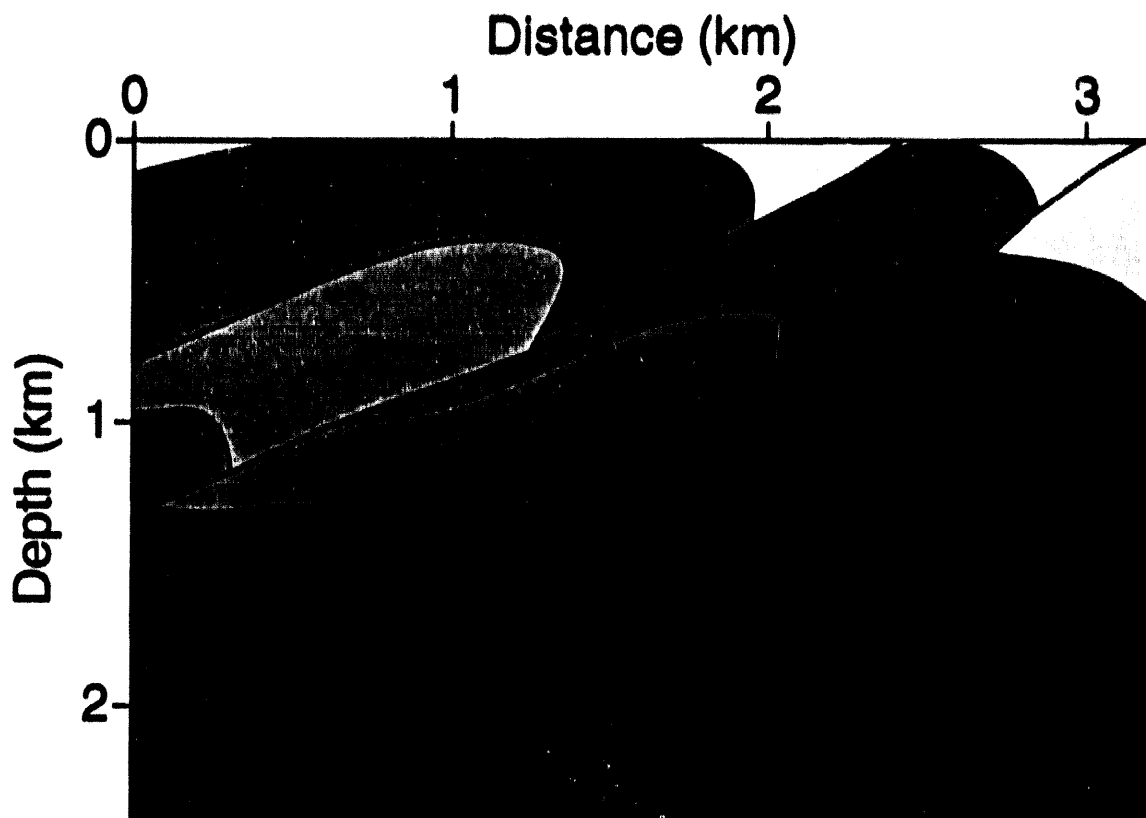


FIG. 5.2. Overthrust model. Within each layer, the seismic velocity increases with depth. Gaussian beam modeling in media of this complexity has not yet been considered in the literature.

Gaussian beams represent high-frequency asymptotic solutions of the wave equation. These solutions are concentrated close to rays. Similar to the classical ray methods, where

the source wavefield is expanded into rays, in the GBM the source field is expanded into Gaussian beams. Several degrees of freedom are available to achieve an accurate expansion:

- the number of beams used in the expansion
- the width of each beam
- the phase-front curvature of each beam.

Phase-front curvature, i.e., the second derivative of traveltime evaluated at the ray, and beam width may vary from beam to beam and must be specified at one point, wherever desired, along the ray. The width and the number of beams determine the beam coverage in the area of interest. Since the wave equation is linear, synthetic seismograms may be computed at any point P in the medium as a weighted sum over all beams.

$$u(P) = \int_{\phi} \Phi(\phi) u_{\phi}(P) d\phi, \quad (5.7)$$

where $u(P)$ is the solution at the receiver, and $u_{\phi}(P)$ is the solution of the beam with take-off angle ϕ , evaluated at P . The common procedure for estimating the complex-valued weighting function $\Phi(\phi)$ is to compare integral (5.7) with the exact solution of the wave equation in homogeneous media for frequency $\omega \rightarrow \infty$ (Červený, et al, 1982). Additionally, it is assumed that, at the source, the phase-front curvature and the width of the beam are the same for all take-off angles or, as considered by Müller (1984), vary linearly as a function of ϕ .

Hale (1991) followed the commonly discussed approach in the literature of setting the curvature of the phase-front of the beam to zero at the source; i.e., phase-fronts are planar at the source. The introduction of beams with plane phase-fronts at the source does not include any error; however, that choice reduces the variety of possible expansions of a wavefield into Gaussian beams. According to equations (5.5) and (5.6), the only parameter left to be specified is ϵ_2 . ϵ_2 specifies the beam width at the source (see Figure 5.3). The source beam width, evaluated at peak-frequency, will be referred to as the *beam parameter*.

To illustrate difficulties inherent to the GBM, a simple experiment is sketched in Figure 5.4. Rays are traced from a single shotpoint and are reflected from an interface at the depth of 2.5 km. Synthetic seismograms for various choices of beam parameter are shown in Figure 5.5. Note that the choice of beam parameter has influence on the generated time sections. Even in this simple model, a poor choice of beam parameter yields spurious arrivals and abnormal amplitude behavior.

This phenomenon may be understood better by considering Figure 5.6. The diagram shows the dominant frequency beam widths at the ray ends as a function of source-to-receiver offset. The wrong choice of beam parameter yields beam widths that are too broad at the ray ends. For the beam parameter of 0.1 km, the width of the beams at the ray ends even exceeds the horizontal dimensions of the model. This leads to spurious arrivals because the influence of the beam is not limited to the vicinity of its

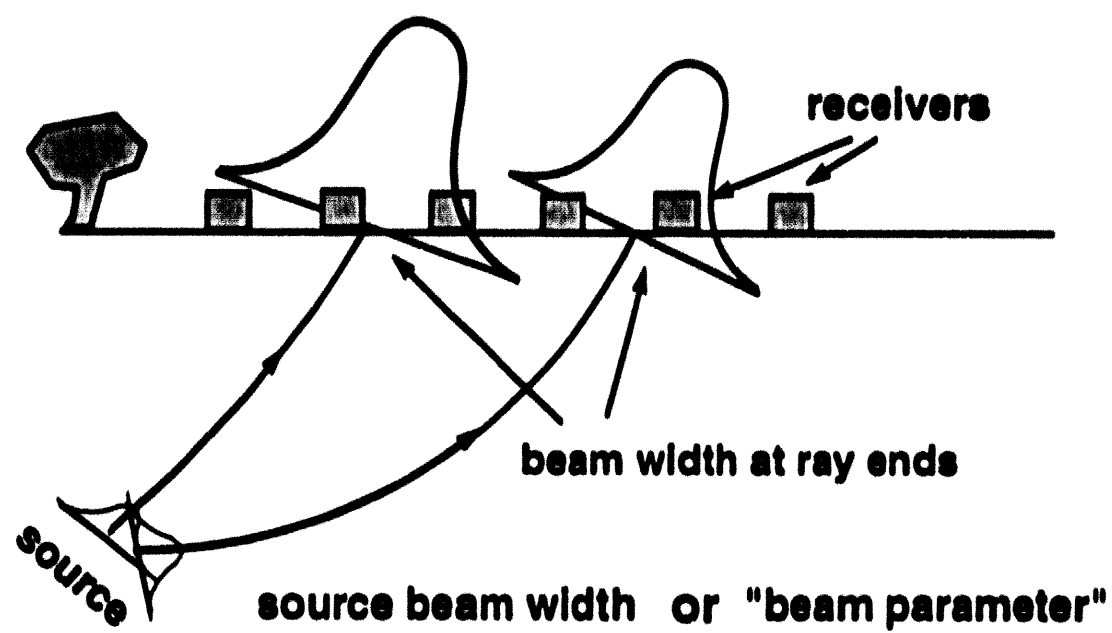


FIG. 5.3. Sketch to illustrate the meaning of *beam parameter* and *beam width at ray end*. Note that the rays are the support of the beams and that the amplitude of a beam decreases exponentially away from the ray. The response at the receivers is obtained as a weighted sum over the beams.

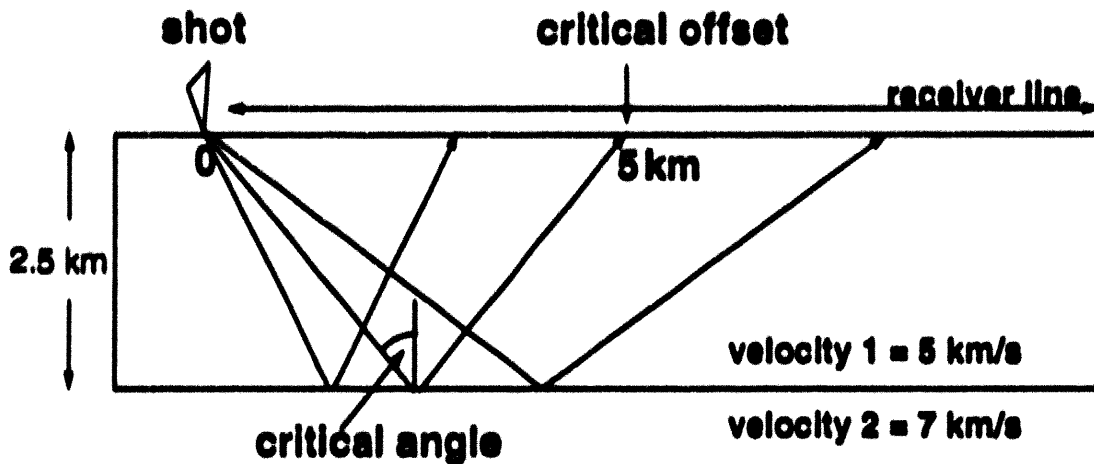


FIG. 5.4. Geometry of an experiment to show the dependence of the GBM results on the choice of beam parameter. Seismic sections for various beam parameters are displayed in Figure 5.5.

emerging point. The seismic section shown in Figure 5.5b was generated for a choice of beam parameter of 1 km. As one can see in Figure 5.6, the widths of the beams at the ray ends are much smaller than in the previous case, hardly exceeding 1.8 km even for large offsets. As expected, the corresponding seismic section looks acceptable. Do these results imply that a larger beam parameter (i.e., a broader beam width at the source) produces more stable results? Analysis of Figures 5.5c and 5.5d proves that this assumption is incorrect. The choice of a 2 km and, more obviously, the choice of 5 km beam parameter again generate spurious arrivals due to very large beam widths at the ray ends. These simple experiments indicate that a proper choice of beam parameter is crucial in generating accurate seismograms. Specifically, if the beam parameter is too small (i.e., the beam is too narrow at the source), a strong spreading of the beam along the ray can be expected.

5.4 Basic Assumptions Inherent to the Beam Approach

From the simple experiments above, we learned that the concentration of the beam along the central ray is essential to generating accurate synthetic seismograms. A brief review of some basic assumptions of the dynamic ray tracing supports this hypothesis:

- The dynamic ray tracing method is based on the eikonal equation. As discussed in Chapter 2, strictly speaking the eikonal equation describes only the high-frequency

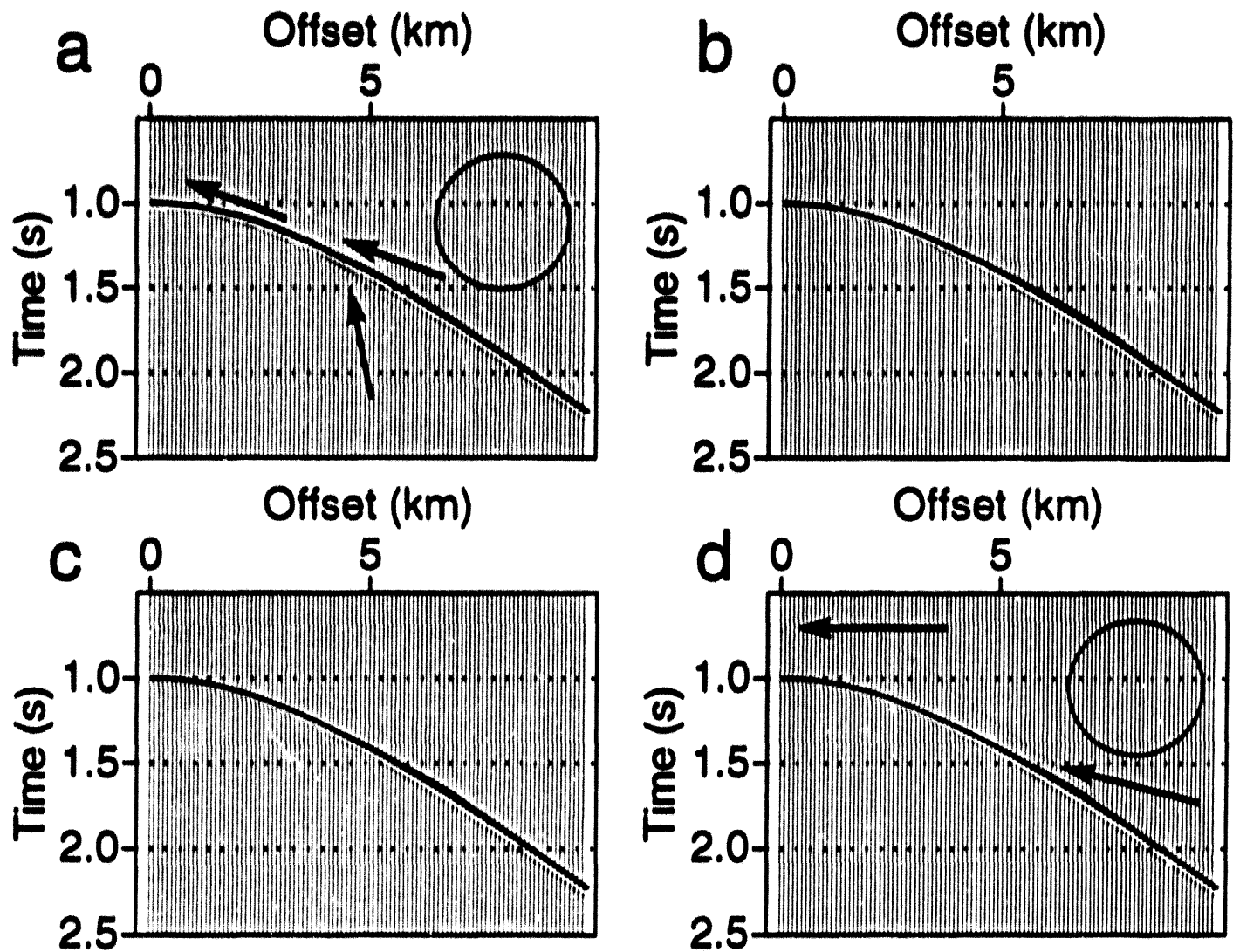


FIG. 5.5. Seismic sections computed for the experiment sketched in Figure 5.4. The choice of beam parameter is the following: (a) 0.1 km; (b) 1.0 km; (c) 2.0 km; (d) 5.0 km. The arrows point to spurious arrivals. Close examination of the encircled areas show artifacts due to the fact that beams have become too broad.

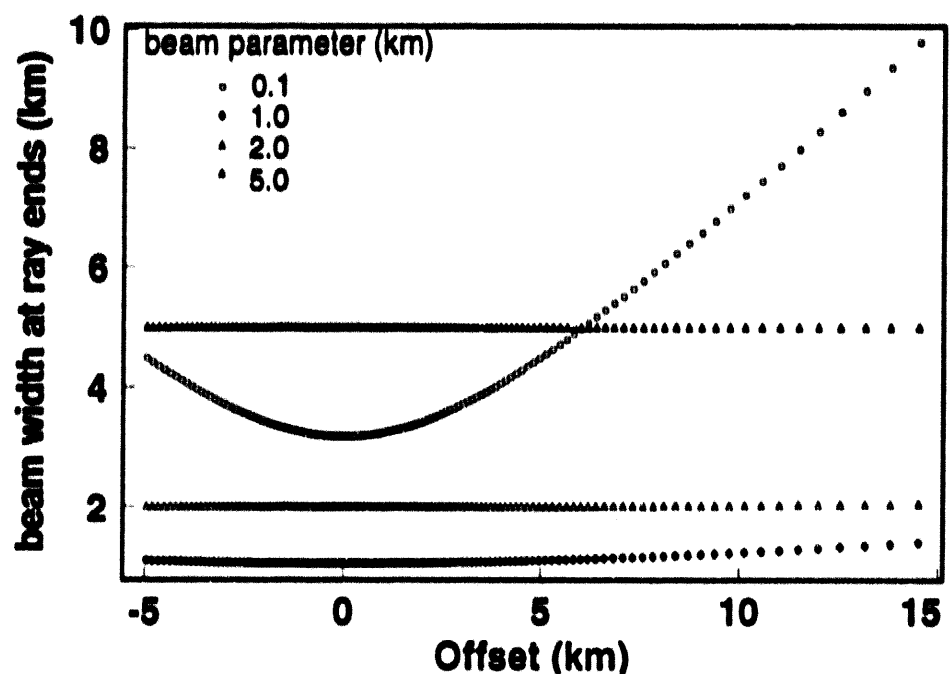


FIG. 5.6. A more detailed analysis of the results obtained in the experiment sketched in Figure 5.4 aids in better understanding of some of the difficulties of Gaussian beam modeling. The diagram displays the dominant-frequency beam width at the receiver as a function of offset. Each symbol denotes a different choice of beam parameter at the source.

part of the wavefield. This assumption is usually stated as the *validity condition* of ray theory:

$$\lambda \ll l ,$$

where λ is the wavelength of the signal and l represents the length scale of the medium (e.g., Bleistein, 1984). Note that large frequencies yield small beam widths (equation (5.4)).

- The traveltime in the neighborhood of a central ray is approximated by a Taylor expansion (equation (2.18)), requiring that the velocity has to vary smoothly relative to the width of the beam. Moreover, velocity discontinuities within the beam width, in general, are not seen by the central ray and yield inaccurate traveltime extrapolations.
- The dynamic ray tracing equation (2.20) has been derived under the paraxial assumption (2.19). In two dimensions, this assumption yields:

$$n \cdot \left(v^{-1} \frac{\partial v}{\partial n} \right)_{n=0} \ll 1 .$$

Even for small values of extrapolation distances n away from the central ray, the paraxial assumption will break down if strong velocity gradients perpendicular to the ray are present in the medium.

In summary, three basic requirements can be stated:

1. The length scale of the medium must be much larger than the wavelength of the wavefield considered.
2. The width of the beam should be as narrow as possible along the ray.
3. The velocity has to vary smoothly relative to the width of the beam.

Only if these three criteria are satisfied will the Gaussian beam method accurately represent the seismic wavefield. The next sections will discuss situations in which one or more of these constraints are violated.

5.5 Gaussian Beams Across Interfaces

Ray tracing in complex subsurface models requires an appropriate transformation of kinematic and dynamic ray tracing data across discontinuities of first- and second- order in velocity. The reflection and transmission of high-frequency Gaussian beams in elastic media has been investigated by Červený and Pšenčík (1984). These authors applied a phase-matching method, i.e., they required the traveltime of incident and reflected or transmitted wave to be equal along a curved reflector.

Hale (1991) traced rays through models containing velocity discontinuities. If a ray impinges on a boundary dividing two media with different velocities or densities, one

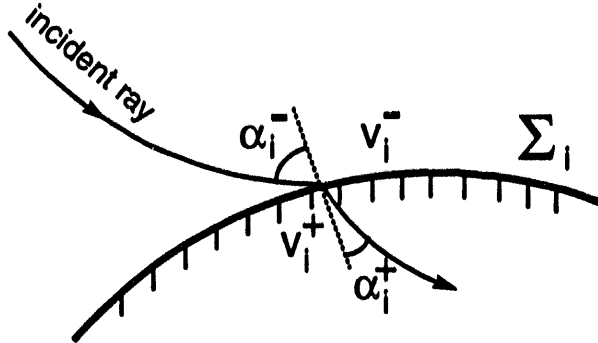


FIG. 5.7. Sketch of the quantities involved in the transmission of a ray at interface Σ_i . The incidence angle is α_i^- , and the refraction angle is α_i^+ . The velocity is discontinuous, jumping from v_i^- to v_i^+ across the interface.

must account for reflection and transmission at boundaries in order to properly calculate the wavefield amplitude. While Hale implemented Červený and Pšenčík's correction for the influence of discontinuities on the geometrical spreading, the loss of energy reflected by impedance discontinuities was not included. I modified the program to compute the necessary correction factor A_{RT} along the ray.

$$A_{RT} = \sum_{i=1}^N R_i \sqrt{(v_i^- / v_i^+) \sqrt{(\cos \alpha_i^+ / \cos \alpha_i^-)}} \quad (5.8)$$

This result is derived in detail in Appendix C. The summation is over all interfaces encountered by the ray. At the i th interface, this expression involves the reflection or transmission coefficient R_i for acoustic pressure waves, which can be evaluated by assuming the continuity of both pressure and the normal component of particle velocity across an interface (Brekhovskikh, 1960). The meaning of the other quantities in equation (5.8) is sketched in Figure 5.7. If the ray is reflected back from interface Σ_i , the two square-roots yield unity because both the velocities and the angles of incident and reflected ray are identical. I also included an option to specify a constant value of density in each geologic block bounded by interfaces. Reflection and transmission coefficients are computed by considering the density discontinuity across the interface. The additional computing time required for evaluating the energy partitioning due to reflection and transmission at interfaces is negligible.

5.6 Near-critical Transmission of Gaussian Beams

There exists a potential danger associated with the transmission of dynamic ray-tracing data. Consider the experiment in Figure 5.8, where rays are traced through a salt dome model. The source is situated at 3.2 km horizontal position. The analysis of the beam width at the ray ends is shown in Figure 5.9. Near-critical rays emerge in the

region of 0 to 1.5 km and yield extremely broad beam widths. The rays reflected from the dome, however, behave well.

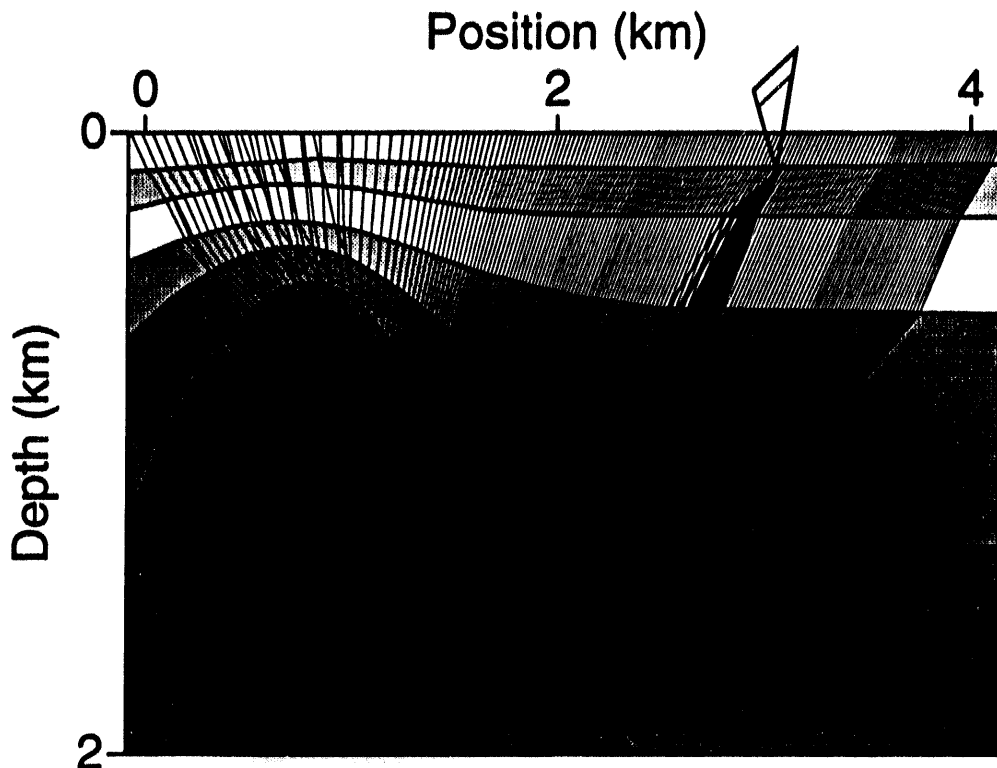


FIG. 5.8. Rays traced in a salt dome model. The source is situated at 3.2 km horizontal position. Near-critical rays emerge in the region of 0 to 1.5 km and yield extremely broad beam widths. As we learned from the example considered in Figure 5.4, these beams will produce spurious arrivals in the corresponding seismic section.

Artifacts due to near critical transmission can be reduced once we better understand the reason for this beam spreading. As derived by Červený and Pšenčík (1984), the dynamic ray tracing quantity q is transformed across interfaces according to

$$q^+ = q^- \frac{\cos(\alpha_i^+)}{\cos(\alpha_i^-)} .$$

For near-critical transmitted rays, α_i^+ is close to $\pi/2$ and the transformed value q^+ will be very small. q^+ , in essence, specifies the new initial beam width on the other side of the discontinuity. According to equation (5.4), a small initial value of q again creates a small initial beam width and, as in the half-space experiment sketched in Figure 5.4, this small initial beam width will produce strong beam spreading!

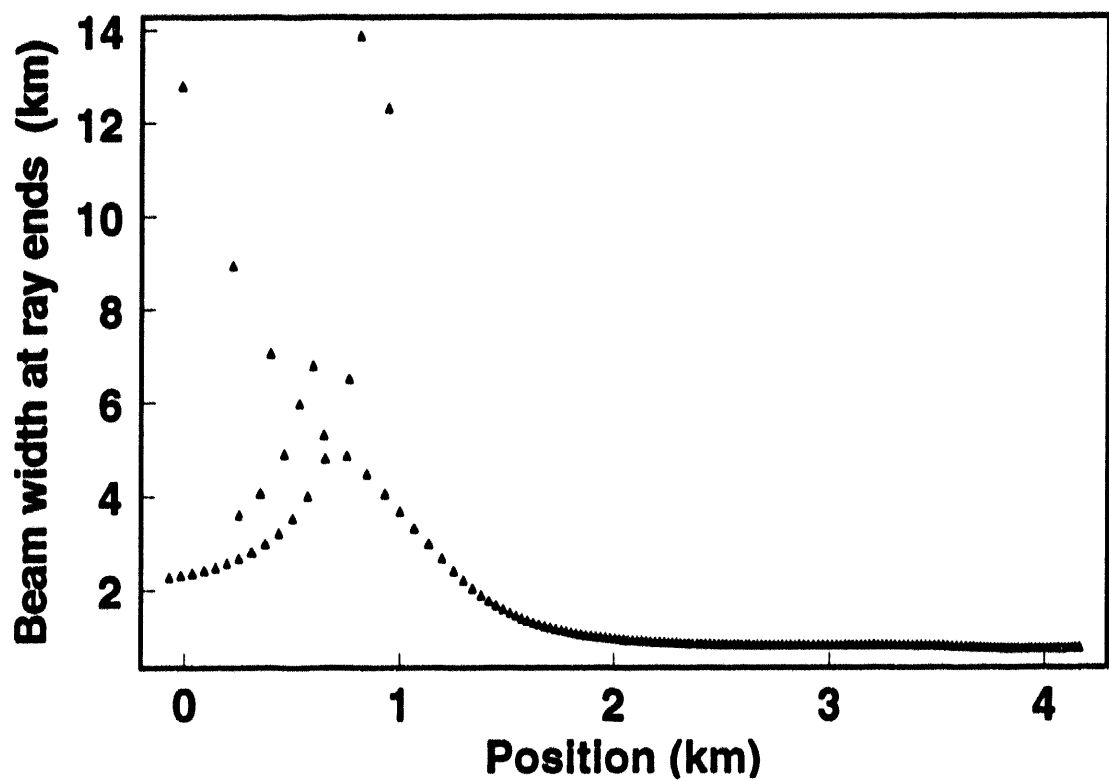


FIG. 5.9. Analysis of the dominant-frequency beam width at the ray ends in Figure 5.8. Data acquired in the region beyond the horizontal position of 1.5 km will yield accurate results.

To avoid spurious arrivals associated with near-critical transmitted rays, I implemented a taper on the transmission coefficients. The amplitudes of these rays are hereby significantly reduced so as not to influence the seismic section.

5.7 The Overthrust Model Experiment

Additional problems can be expected if we trace rays through media such as the overthrust model introduced in Figure 5.2. This model is composed of geologic blocks with different seismic velocities. In each layer, the velocity is increasing with depth. Note that interfaces with strong curvature and sharp edges are present in the model.

The complexity of the medium can be visualized better by displaying rays and wavefronts for a shot situated at 1.15 km horizontal position (see Figure 5.10). White lines show rays that are reflected from the bottom of the model and emerge at the surface. These rays are the only ones chosen to contribute to seismic data collected at the surface. Energy that propagated out of the model is simply represented by black wavefronts, with the corresponding rays deleted. Of the 600 rays traced through this model, less than one-sixth of them end up at the surface; the others either stop at the boundary of the model or they are overcritically incident at velocity discontinuities. In the large shadow zones such as the one between 1.2 km and 1.7 km horizontal position, synthetic data generated by a classical ray-theoretical approach would not show any seismic response.

To test synthetic data computed for this model, Hale (1991) generated a synthetic midpoint gather for the midpoint at 1.6 km, shown in Figure 5.11. Negative and positive offset represent the interchange of source and receiver positions. Reciprocity requires that trace amplitudes be independent of this interchange. The asymmetry in the figure indicate, that the reciprocity in the created dataset is violated, so that the data are not accurate. Hale supposed two reasons for the failure. First, the missing correction for reflection and transmission on the amplitudes, and, second, the violation of the beam assumption. The latter requires the model parameters to vary smoothly relative to the width of the beam (e.g., White, et al., 1987). At an interface, for example, the width of the beam has to be significantly smaller than the radius of curvature of the interface.

Figure 5.12 displays the result of the common midpoint gather after correcting for the energy loss due to reflection and transmission. The asymmetry is still strong, and one cannot recognize any improvement. I evaluated the beam width at the surface for a source located at a horizontal distance of 1.6 km (see Figure 5.13). The range of beam widths exceeds the dimensions of the model by about one order of magnitude! This indicates that beams attached to rays do not provide an accurate description of the wavefield. Moreover, I was unable to choose *any* beam parameter that gave acceptable beam widths at the surface.

5.8 Application of Gaussian Beam Modeling In Complex Media

Increasing the complexity of the model will eventually violate the basic assumptions of the GBM laid out in Section 5.4. Complex media such as the overthrust model shown

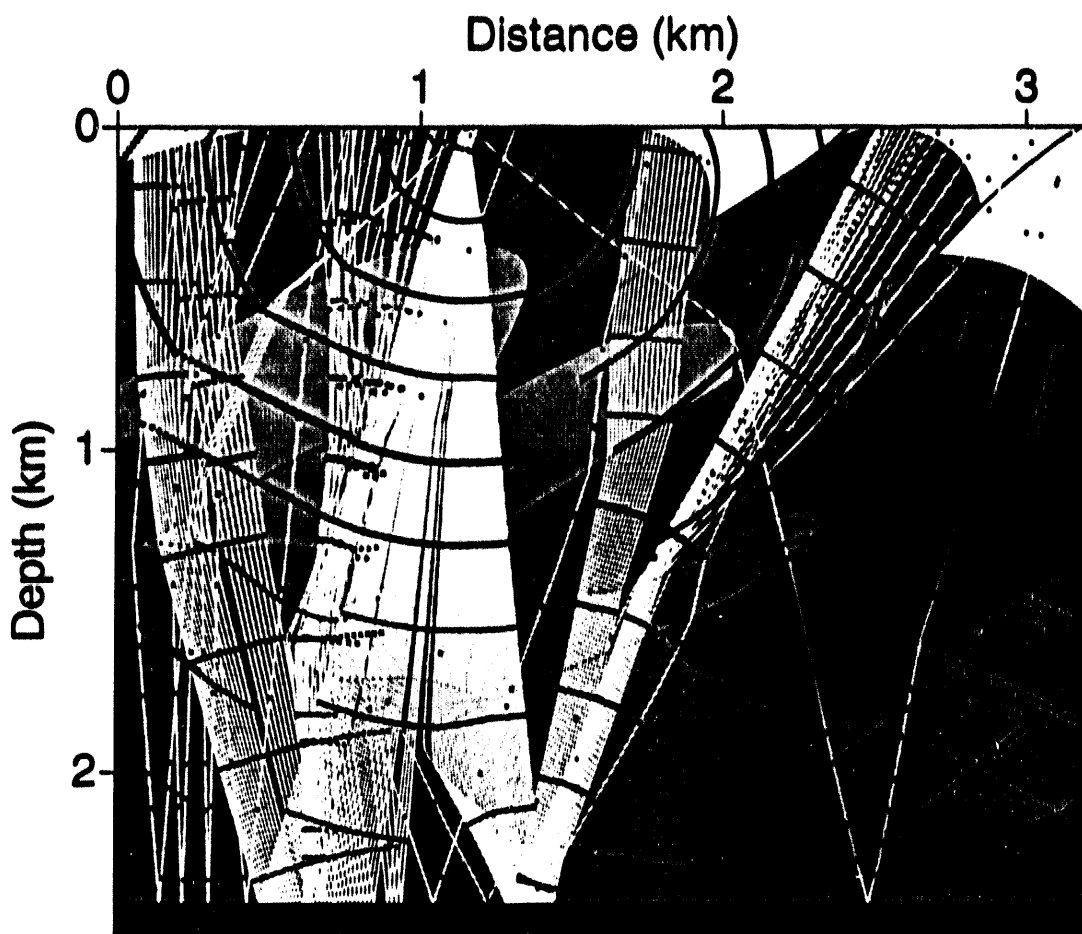


FIG. 5.10. Rays and wavefronts for a shotpoint situated at 1.15 km horizontal position in the overthrust model (Figure 5.2). White lines show rays that are reflected from the bottom of the model and emerge at the surface. Energy that propagates out of the model is represented by black wavefronts only, with the corresponding rays deleted.

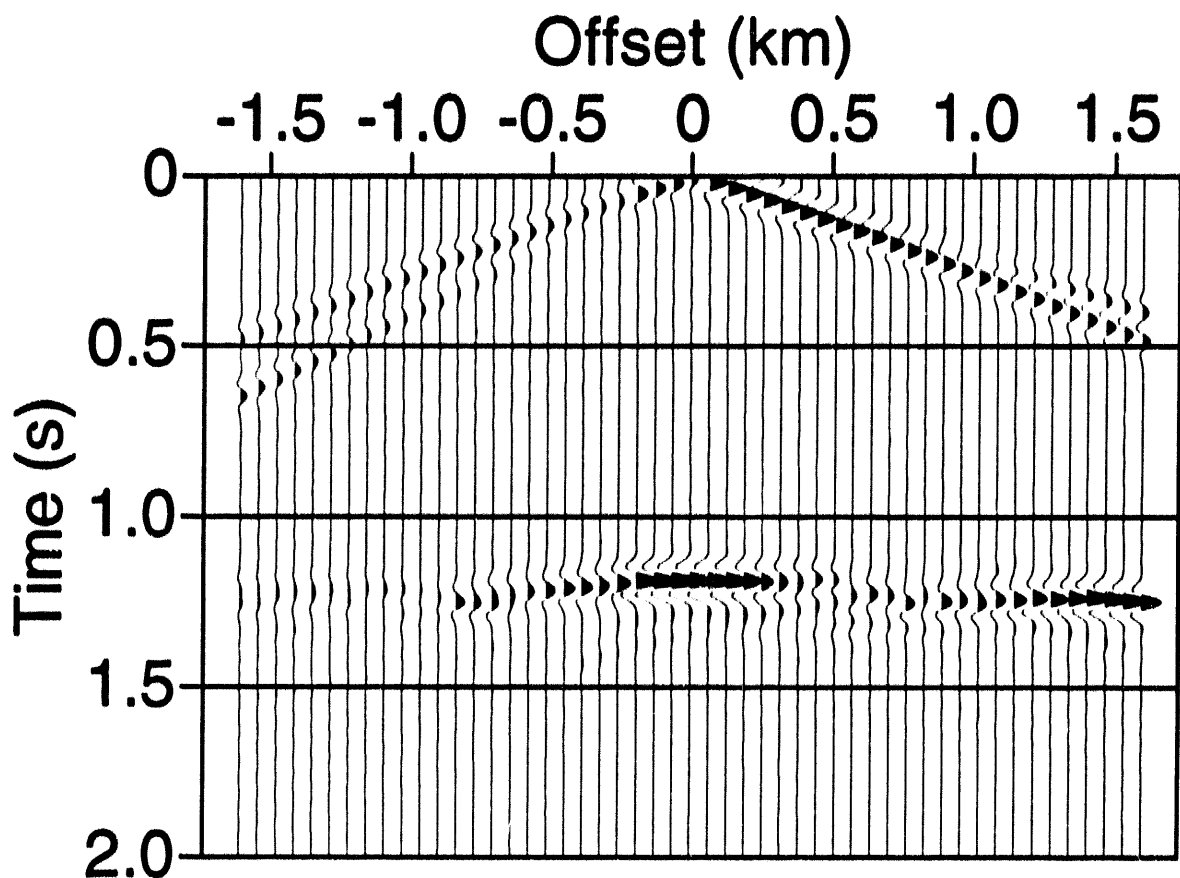


FIG. 5.11. Common midpoint gather for the model shown in Figure 5.2. The midpoint is situated at 1.6 km offset. Negative and positive offset represent the interchange of source and receiver positions. The asymmetry suggests that the data generated fail to satisfy reciprocity. In this section, the correction for transmission and reflection of seismic energy at velocity discontinuities is not included.

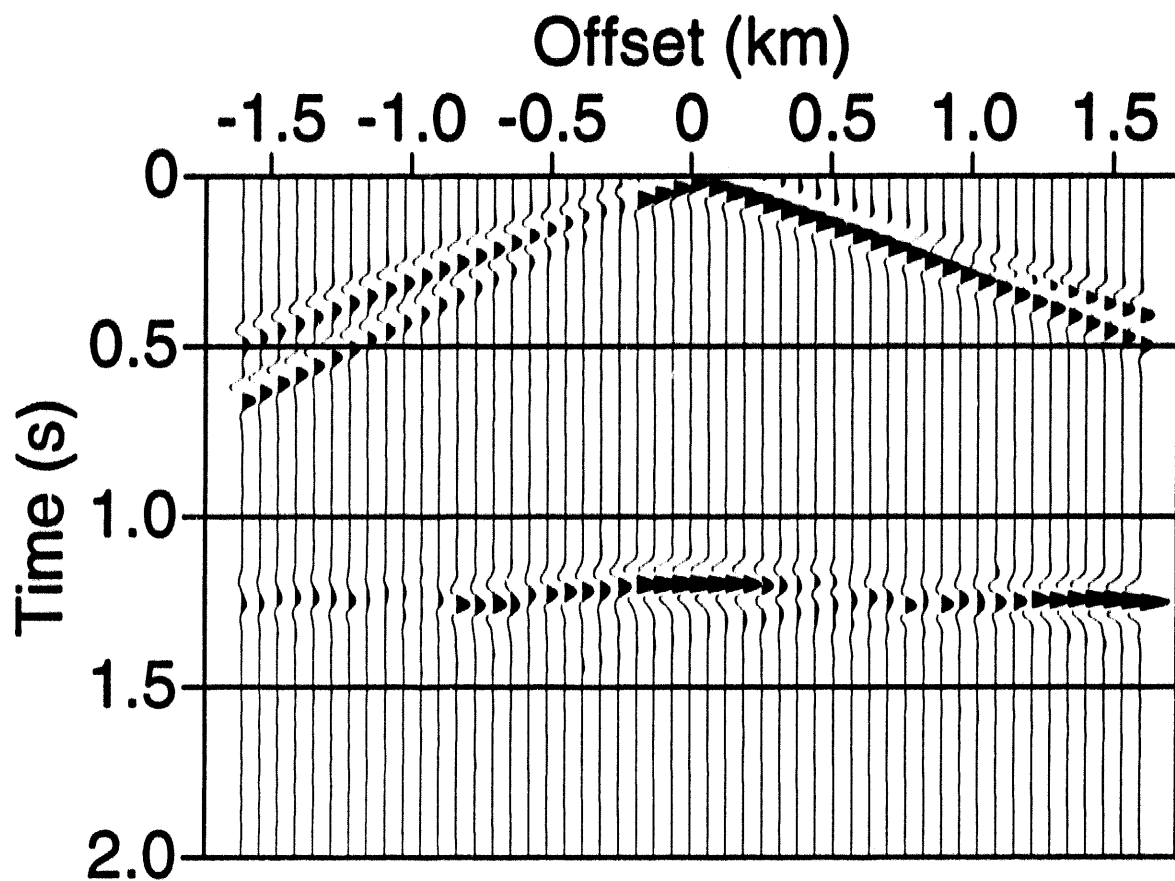


FIG. 5.12. Common midpoint gather for the model shown in Figure 5.2. The midpoint is situated at 1.6 km offset. This section differs from that in Figure 5.11 only in that the correction for transmission and reflection of seismic energy at velocity discontinuities is now included. The asymmetry, however, remains.

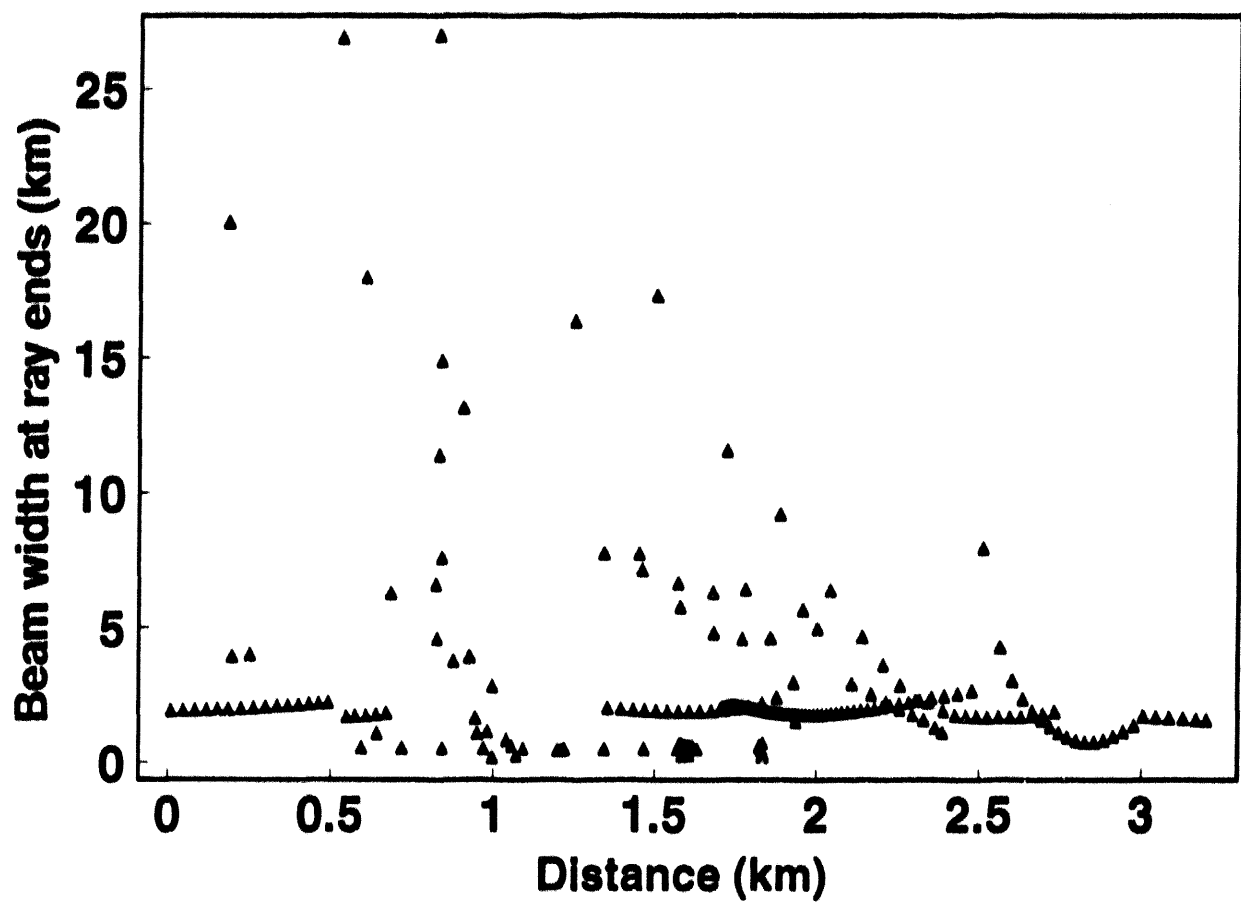


FIG. 5.13. Analysis of the dominant frequency beam widths at the ray end indicates the violation of the beam assumptions for the overthrust model (Figure 5.2). Several beam widths exceed the horizontal dimension of the model by about one order of magnitude.

above certainly violate these assumptions; thus we should not be surprised to encounter discouraging test results. The question is whether we can apply some means to reduce disturbing artifacts and generate more stable results.

I suggest a compromise between the rigorous validity conditions of the beam method and the practical application of beam modeling. Three criteria should be carefully examined when modeling seismic responses in complex media:

- The complex traveltime should not be extrapolated too far away from the central ray. More specifically, the range of extrapolation should not exceed the natural length scale of the medium. Receivers should add up contributions from only nearby emerging beams.
- The beam width should not be fixed at the source. In complex media, each beam eventually encounters a different velocity field and thus requires an individual *optimal* beam parameter. This beam parameter must be chosen such that the beam remains as narrow as possible along the ray. Both the location at which to assign this parameter (e.g., at the source or at the ray ends) and its optimum value have been investigated by various authors (Weber, 1988; Müller, 1984; Červený, 1985a,b). The published results, however, were satisfactory only for models with minor inhomogeneities (Kästner and Fritzsche, 1988). I tested the approach suggested by Červený (1985b) and found some encouraging results which I present below.
- Each receiver should receive contributions from several beams. As suggested by Beydoun and Keho (1987), the GBM generally requires on the order of 10 beams in the vicinity of the receiver in order to reconstruct the high-frequency part of the wavefield.

To analyze the importance of the first criterion, I performed the reciprocity test for the overthrust model, but this time I allowed only nearby beams to contribute to the receivers. One cannot avoid that some beams spread too much, however, their contribution to the seismic section can be reduced by this means. Figure (5.14) shows a synthetic midpoint gather for the midpoint at 1.6 km horizontal position and a limited extrapolation range of 0.32 km. Only beams with their central ray situated closer than 0.32 km from the receiver contribute to the generated seismic data. The symmetry of the synthetic midpoint gather indeed improved. The asymmetric direct-arrival branches disappeared and noisy artifacts between 1.0 and 1.5s arrival time have vanished. The characteristics of the reflections from the bottom of the model, however, remain essentially unchanged. The latter suggests that the reflected energy is still influenced by broad beams.

As mentioned above, I used an optimal choice of beam parameter to generate the midpoint gathers. The optimal choice is based on a statistical analyses of the dynamic ray tracing data evaluated at the ray ends. The optimal choice is the one that on average produces the minimum beam width at the surface. This analysis is cumbersome and one would like to have an automatic procedure to compute accurate seismic data.

The approach proposed by Červený (1985b) does not require the determination of an optimal beam parameter. Here, based on Červený's empirical results rather than on

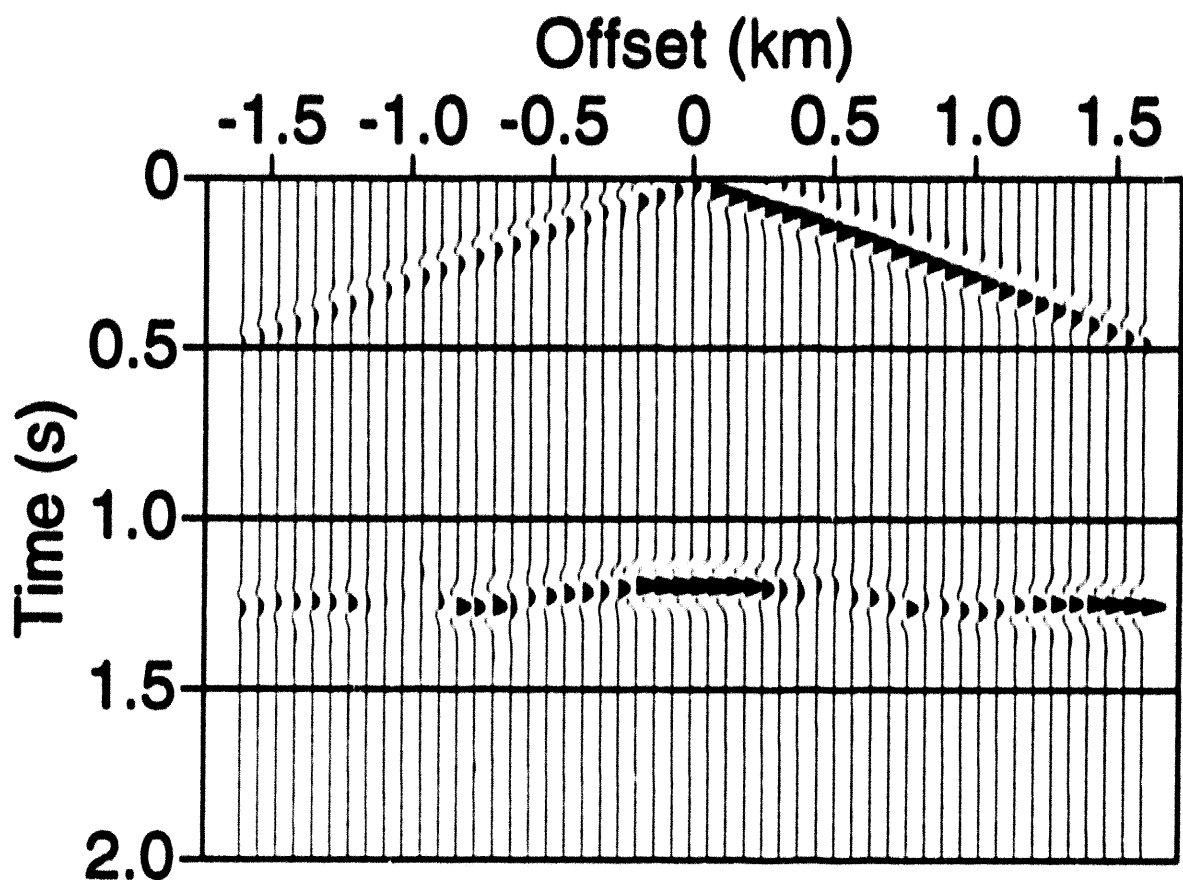


FIG. 5.14. Common midpoint gather for the model shown in Figure 5.2. The midpoint is situated at 1.6 km horizontal position. Only beams with their central ray situated closer than 0.32 km from the receiver contribute to the generated seismic data. The asymmetric direct arrival branches and noisy artifacts between 1.0 and 1.5s arrival time vanished. The characteristics of the reflections from the bottom of the model, however, remain unchanged.

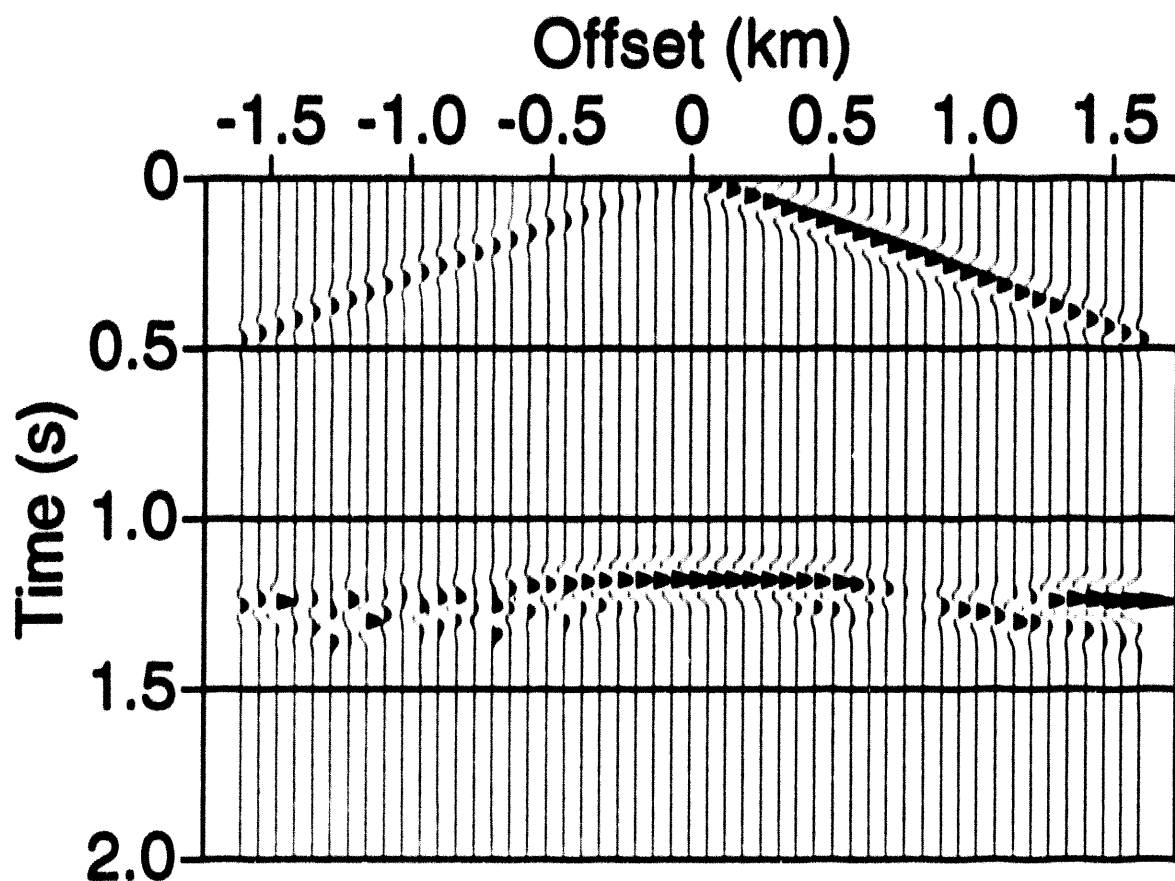


FIG. 5.15. Common midpoint gather for the model shown in Figure 5.2. The midpoint is situated at 1.6 km horizontal position. Only beams with their central ray situated closer than 0.32 km from the receiver contribute to the generated seismic data. The beam widths are chosen for each beam individually as a function of the dynamic ray tracing data q_1, q_2, p_1, p_2 .

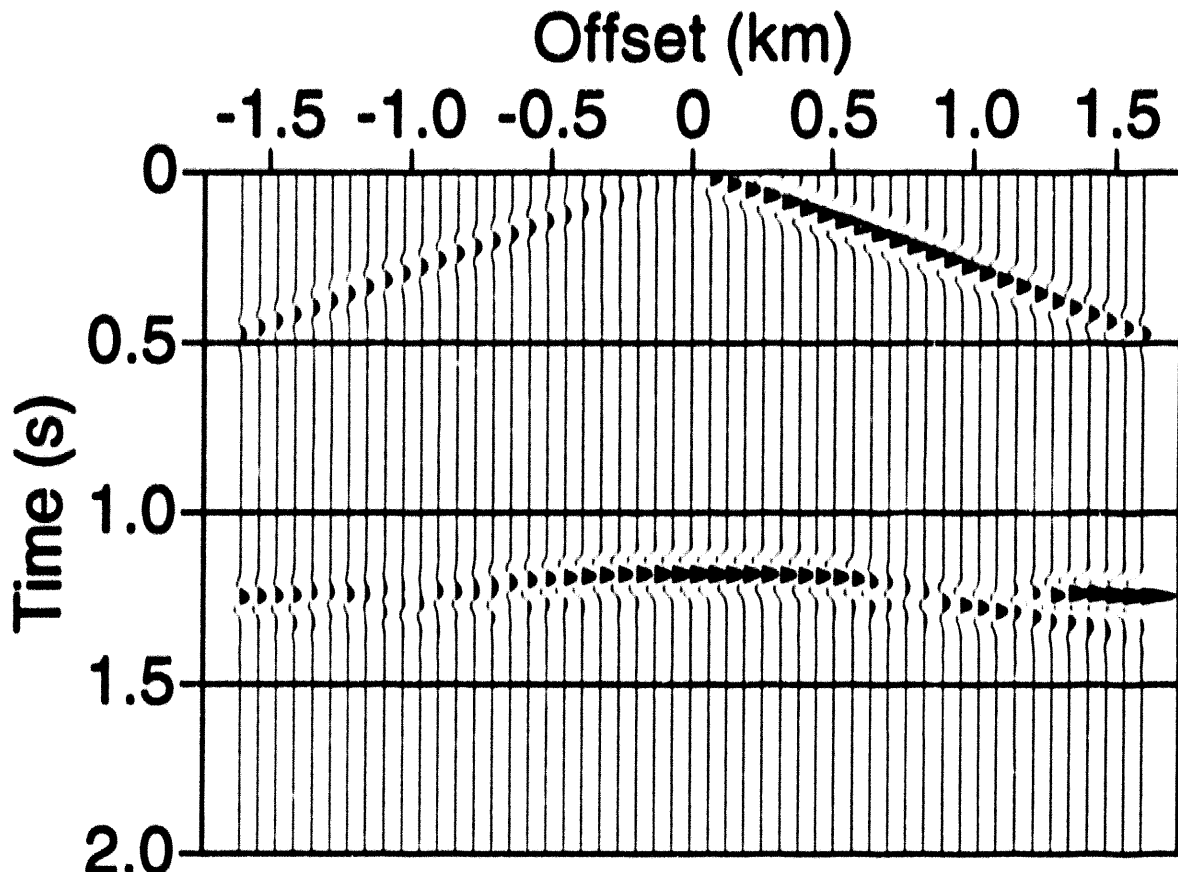


FIG. 5.16. Common midpoint gathers for the model shown in Figure 5.2. The midpoint is situated at 1.6 km horizontal position. Only beams with their central ray situated closer than 0.32 km from the receiver contribute to the generated seismic data. The beam widths are chosen for each beam individually as a function of the dynamic ray tracing data q_1, q_2, p_1, p_2 . Increasing the number of rays traced through the model by a factor of five (as compared with the rays shown in Figure 5.10) improves the continuity of the recorded seismic reflections.

theoretical derivations, the beam widths are chosen for each beam individually as a function of the dynamic ray tracing data q_1, q_2, p_1, p_2 . The function $\Phi(\phi)$ responsible for an appropriate weighting of the beams is approximately derived by an asymptotic evaluation of integral (5.7), followed by a comparison with ray-theoretical results. I implemented this idea of automatically prescribing the beam width. The resulting midpoint gather in Figure (5.15) is quite symmetric; however, at least two features are still disturbing. First, the direct arrivals corresponding to negative offsets are weaker than the ones corresponding to positive offsets. The offset is negative if the receiver is situated on the right side of the midpoint. Rays traveling near horizontal from right to left are overcritically incident on velocity discontinuities and are not propagated further (recall from Chapter 2 that the geometrical optics approach does not handle the propagation of headwaves). This is the reason why far more direct rays emerge at receivers with positive offset. Second, the reflections from the bottom of the model are erratic for the offsets between -1.5 km and -0.5 km. A closer examination of the contributing central rays reveals that only very few rays contribute to these offsets. Moreover, most of these rays went through caustics of the wavefield and produce phase shifts. This situation violates the third criterion established in this section. In fact, as seen in Figure (5.16), increasing the number of rays traced through the model by a factor of 5 (as compared to the rays shown in Figure 5.5) improves the continuity of the recorded seismic reflections.

It is not my intention to overestimate the accuracy of the results generated by applying the three criteria outlined above. In particular, the tools suggested to improve the results are based on experience rather than on a strict mathematical basis. However, in my subjective opinion, the means proposed to increase the data quality yield satisfactory reciprocity in the generated common midpoint gathers, indicating that the computed seismic sections are more accurate. This is especially evident if one recalls that the basic assumption of the GBM are severely violated in the model considered.

5.9 Quo Vadis Gaussian Beams?

Research on Gaussian beams started approximately 10 years ago with the prospect of solving many problems inherent to classical ray theory. Few authors highlighted the ambiguity associated with a freely varying beam-width parameter. In practice, this parameter has been defined somewhat arbitrarily, mainly adjusted to minimize errors in the beam superposition (Klimeš, 1989) or tuned to minimize errors associated with velocity inhomogeneities (Kästner and Fritsche, 1988). Despite these efforts, the results published in the literature are limited to models with simple velocity structures; none of the references provides modeling results for media with complexity comparable to that of the overthrust model shown here.

In the previous section, I suggested a procedure to avoid some of the artifacts associated with the beam-spreading problem. However, only a more theoretical derivation has the potential of actually solving this difficulty.

Based on my experience with the Gaussian beam procedure, I suggest two main directions for future research which might help to improve the performance of Gaussian

beam modeling:

- A more sophisticated choice of beam parameter has to be developed. The parameter determining the beam width could for example be related to the physical concept of Fresnel volumes. However, it might then be necessary to specify a different beam parameter (specifying the phase-front curvature and beam width) at well chosen locations along each ray, that is, as a function of ϕ . In addition, we should consider a weighting function that varies with ϕ , that is, $\Phi(\phi)$ in equation (5.7) must be evaluated.
- Smoothing of the velocity field could reduce the spreading problem of the beams. This approach is motivated by the good performance of the Gaussian beam migration procedure (e.g., Hill, 1990; Hale, 1992), where model velocities are smoothed.

Chapter 6

CONCLUSION

6.1 Summary

The purpose of this research has been to enhance the usefulness of the dynamic ray tracing procedure both for modeling of seismic responses and for interpretation of previously acquired data. Several new implementations to the dynamic ray tracing software have been introduced to improve the flexibility and accuracy of the proposed modeling method.

The modeling software GBmod now allows the introduction of a broader class of raypaths. For example, it is now possible to trace multiples in surface or VSP experiments. Additionally, I added options to include attenuation and density variations. The influence of energy partitioning at interfaces and of 3-D geometrical spreading in 2-D models can now be simulated efficiently. A new feature called Fresnel-volume ray tracing has been included to study the resolution and the validity conditions of ray-theoretical methods. All these modifications can be used while maintaining the attractive feature of computational speed and limited computer storage.

The Gaussian beam method (GBM), one important application of the dynamic ray-tracing procedure, has been studied in Chapter 5. The theory of beam modeling is accurate and efficient as long as models with only weak inhomogeneities are considered. A simple experiment and a summary of the intrinsic assumptions of the GBM help to understand difficulties when applying the method to more complex velocity structures. The GBM, as currently developed, cannot properly handle models of high complexity. The limitations are similar to those of classical ray theory. However, I proposed some useful criteria to avoid most of the artifacts associated with the violation of the beam assumptions.

Modeling using GBM is only one possible application of the dynamic ray-traced data generated along the ray. Alternative methods (e.g., the paraxial methods) can also use these data to create synthetic seismograms. The new modifications such as the tracing of multiples, computation of out-of-plane spreading, or reflection and transmission correction are evaluated independently of the Gaussian beam procedure.

6.2 Future Work

The GBM will be used for modeling of seismic wavefields in models with significant inhomogeneities only when we achieve a focusing of the beams along the ray. In this case, an extension of the GBM modeling code to elastic media would be worthwhile. The required changes are not difficult. An interactive procedure for the modeling and a more

involved extension to three-dimensional models could then be considered.

The extension to three dimensions is useful not only for modeling of seismic data by the Gaussian beam procedure. New methods designed to efficiently simulate seismic wavefields in triangulated subsurface models such as wavefront tracing (e.g., Coultrip, 1993) could be considered and extended to three-dimensional media, as well.

Appendix A

SOLUTION OF THE TWO-DIMENSIONAL DYNAMIC RAY TRACING EQUATIONS

The dynamic ray tracing system (2.26)

$$\frac{dq}{d\sigma} = p \quad , \quad \frac{dp}{d\sigma} = -\frac{1}{v^3} v_{,11} q ; \quad (\text{A-1})$$

can be solved analytically in media with a constant gradient in $1/v^2$, i.e., the sloth can be represented in the form:

$$v^{-2}(x, z) \equiv s(x, z) = s_{00} + s_{,x}x + s_{,z}z. \quad (\text{A-2})$$

Hale (1991) used a symbolic computer language to verify the following solutions for the coupled system of differential equations (A-1):

$$\begin{aligned} q(\sigma) &= \frac{1}{\sqrt{s_0 s}} \left\{ \left[s_0 + \frac{s_1(\sigma - \sigma_0)}{2} \right] [q(\sigma_0) + p(\sigma_0)(\sigma - \sigma_0)] \right. \\ &\quad \left. + \left(\frac{s_1^2}{4s_0} - s_2 \right) q(\sigma_0)(\sigma - \sigma_0)^2 \right\} ; \\ p(\sigma) &= \frac{1}{\sqrt{s_0 s}} \left\{ [s_0 + s_1(\sigma - \sigma_0)] p(\sigma_0) + \left[\frac{s_1}{2} + \left(\frac{s_1^2}{2s_0} - 2s_2 \right) (\sigma - \sigma_0) \right] q(\sigma_0) \right\} \\ &\quad - \left[\frac{s_1 + 2s_2(\sigma - \sigma_0)}{2s} \right] q(\sigma) , \end{aligned} \quad (\text{A-3})$$

where s_0 , s_1 , and s_2 are constants defined by :

$$\begin{aligned} s_0 &\equiv s[x(\sigma_0), z(\sigma_0)] , \\ s_1 &\equiv s_{,x}p_x(\sigma_0) + s_{,z}p_z(\sigma_0) , \\ s_2 &\equiv \frac{1}{4} (s_{,x}^2 + s_{,z}^2) , \end{aligned}$$

so that

$$s = s[x(\sigma), z(\sigma)] = s_0 + s_1(\sigma - \sigma_0) + s_2(\sigma - \sigma_0)^2.$$

For a given set of initial conditions $q(\sigma_0)$ and $p(\sigma_0)$, (A-3) can be used to obtain the dynamic ray-tracing data at any value of σ . In the ray-tracing part of the modeling, the quantities $q(\sigma)$ and $p(\sigma)$ need only be evaluated for the intersections with triangle edges. To continue the dynamic ray tracing, q and p are transformed across the interface by

applying a phase-matching procedure. The transformed values then serve as new initial conditions for system (A-1).

Appendix B

MATRIX Q AND ITS RELATION TO THE RAY JACOBIAN

In classical ray theory, geometrical spreading is described by ray Jacobian J . In three dimensions, the Jacobian is a measure of the cross-sectional area of a ray tube. Due to the choice of coordinate systems introduced in Chapter 2 (recall that our monotonically increasing parameter along the ray is σ and not the arclength s), a strict derivation of the relation between the matrix Q and the ray Jacobian is necessary.

Assume a family of four rays $\Omega(\gamma_1, \gamma_2)$, $\Omega(\gamma_1 + \delta\gamma_1, \gamma_2)$, $\Omega(\gamma_1, \gamma_2 + \delta\gamma_2)$ and $\Omega(\gamma_1 + \delta\gamma_1, \gamma_2 + \delta\gamma_2)$ forming a ray tube for a fixed value of σ (Figure B-1). The ray parameters γ_1 and γ_2 can for example be identified as the takeoff angle and the azimuth of the ray.

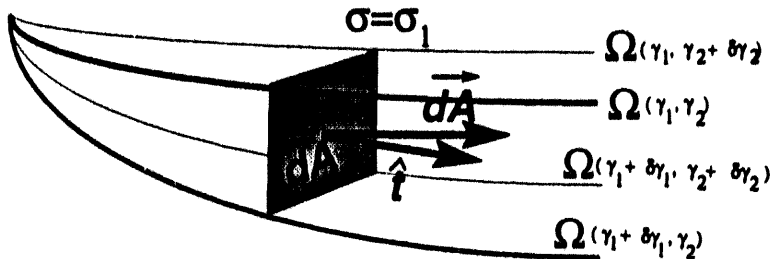


FIG. B-1. A ray tube formed by a family of four rays. dA represents a cross-sectional area spanned by the rays for a fixed value of σ . To obtain the corresponding cross-sectional surface area for fixed value of traveltime τ , one has to project the vectorial surface element $d\vec{A}$ onto the tangent \hat{t}

The vectorial surface element $d\vec{A}$ is projected onto the tangent \hat{t} to obtain the corresponding cross-sectional surface area for a fixed value of traveltime τ . This area can be considered a differential element of the wavefield and is directly related to the geometrical spreading.

As shown in Bleistein (1984), the differential subsurface element $d\vec{A}$ can be expressed as

$$d\vec{A} = \left(\frac{\partial x_i}{\partial \gamma_1} \times \frac{\partial x_j}{\partial \gamma_2} \right)_{\sigma=\sigma_1} d\gamma_1 d\gamma_2,$$

where \times denotes the cross product. The magnitude of this vector represents the differential area dA . The area $dA^{(\tau)}$, i.e., the area corresponding to a fixed value of traveltime

can be simply evaluated by using the dot-product:

$$\begin{aligned} dA^{(r)} &= d\vec{A} \cdot \hat{t} = \left(\frac{\partial x_i}{\partial \gamma_1} \times \frac{\partial x_j}{\partial \gamma_2} \right)_{\sigma=\sigma_1} d\gamma_1 d\gamma_2 v \frac{\partial x_i}{\partial \sigma} \\ &= v \left| \frac{\partial(x_1, x_2, x_3)}{\partial(\gamma_1, \gamma_2, \sigma)} \right| d\gamma_1 d\gamma_2 . \end{aligned}$$

Using the definition of the ray Jacobian, $dA^{(r)} = J d\gamma_1 d\gamma_2$, yields

$$J = v \left| \frac{\partial(x_1, x_2, x_3)}{\partial(\gamma_1, \gamma_2, \sigma)} \right| = v \det(\mathbf{T}) .$$

\mathbf{T} , the transformation matrix from ray parameters to the cartesian system, can be expressed by

$$\mathbf{T} = \mathbf{H} \cdot \hat{\mathbf{Q}} ,$$

where

$$\mathbf{H} = \left(\frac{\partial(x_1, x_2, x_3)}{\partial(q_1, q_2, s)} \right) \quad \hat{\mathbf{Q}} = \left(\frac{\partial(q_1, q_2, s)}{\partial(\gamma_1, \gamma_2, \sigma)} \right) .$$

Both the cartesian and the ray-centered coordinate systems are orthogonal; thus $\det \mathbf{H} = 1$. $\hat{\mathbf{Q}}$ is a (3×3) matrix with the upper left (2×2) submatrix representing the matrix \mathbf{Q} calculated during the dynamic ray tracing. In other words, the Jacobian J can be written as:

$$\begin{aligned} J &= v \det \begin{pmatrix} \frac{\partial q_1}{\partial \gamma_1} & \frac{\partial q_1}{\partial \gamma_2} & \frac{\partial q_1}{\partial \sigma} \\ \frac{\partial q_2}{\partial \gamma_1} & \frac{\partial q_2}{\partial \gamma_2} & \frac{\partial q_2}{\partial \sigma} \\ \frac{\partial s}{\partial \gamma_1} & \frac{\partial s}{\partial \gamma_2} & \frac{\partial s}{\partial \sigma} \end{pmatrix} \\ &= v \det \begin{pmatrix} \frac{\partial q_1}{\partial \gamma_1} & \frac{\partial q_1}{\partial \gamma_2} & 0 \\ \frac{\partial q_2}{\partial \gamma_1} & \frac{\partial q_2}{\partial \gamma_2} & 0 \\ 0 & 0 & \frac{\partial s}{\partial \sigma} \end{pmatrix} \\ &= v \cdot \frac{\partial s}{\partial \sigma} \cdot \det \begin{pmatrix} \frac{\partial q_1}{\partial \gamma_1} & \frac{\partial q_1}{\partial \gamma_2} \\ \frac{\partial q_2}{\partial \gamma_1} & \frac{\partial q_2}{\partial \gamma_2} \end{pmatrix} \\ &= \det \mathbf{Q} . \end{aligned} \tag{B-1}$$

Relation (B-1) is important in calculation of the amplitudes along each individual ray. The geometrical spreading can be simply evaluated by forming the determinant of the dynamic ray tracing matrix \mathbf{Q} . Note that the sign of J may be different at different sections along a ray separated by caustics. (B-1) will also be used to evaluate the energy loss due to out-of-plane spreading.

Appendix C

TRANSFORMATION OF GAUSSIAN BEAM AMPLITUDES ACROSS INTERFACES

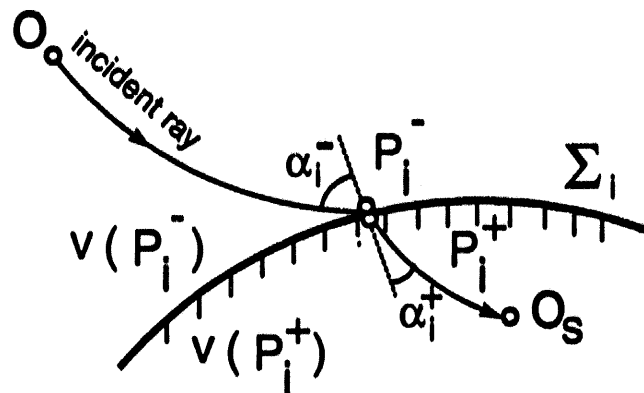


FIG. C-1. Sketch of the quantities involved in the transmission of a beam at interface Σ_i . The incidence angle of the central ray at point P_i^+ is α_i^- , and the refraction angle is α_i^+ . The velocity is discontinuous, jumping from $v(P_i^-)$ to $v(P_i^+)$ across the interface.

Figure C-1 sketches the situation depicting the influence of a curved first order discontinuity on the amplitude of a high-frequency acoustic Gaussian beam. The notation is similar to that used in Chapter 5. Let us first consider the case in which the central ray of a Gaussian beam interacts with one interface Σ_1 . The expression for the ray theoretical amplitude between two points O and P_1^- has been derived in Chapter 4 and is of the form:

$$U(P_1^-) = U_0 \cdot \sqrt{\frac{v(P_1^-)}{v(O)}} \sqrt{\frac{q(O)}{q(P_1^-)}} .$$

Boundary conditions have to be applied to transform the amplitudes across the interface

$$U(P_1^+) = U(P_1^-) \cdot R_1 ,$$

where R_1 denotes the acoustic reflection or transmission coefficient at the interface. If we continue the ray tracing to point O_s , we find:

$$\begin{aligned} U(O_s) &= U(P_1^+) \sqrt{\frac{v(O_s)}{v(P_1^+)}} \sqrt{\frac{q(P_1^+)}{q(O_s)}} ; \\ &= U_0 \cdot \sqrt{\frac{v(P_1^-)}{v(P_1^+)}} \sqrt{\frac{q(P_1^+)}{q(P_1^-)}} R_1 \sqrt{\frac{v(O_s)}{v(O)}} \sqrt{\frac{q(O)}{q(O_s)}} . \end{aligned}$$

This result may be generalized by introducing n curved interfaces:

$$U(O_s) = U_0 \cdot \sqrt{\frac{v(O_s)}{v(O)}} \sqrt{\frac{q(O)}{q(O_s)}} \cdot \prod_{i=1}^n \left(R_i \sqrt{\frac{v(P_i^-)}{v(P_i^+)}} \sqrt{\frac{q(P_i^+)}{q(P_i^-)}} \right) . \quad (\text{C-1})$$

Červený and Pšenčík (1984) derived the expression for the transformation of q across interfaces.

$$q(P_i^+) = q(P_i^-) \cdot \frac{\cos(\alpha_i^+)}{\cos(\alpha_i^-)} . \quad (\text{C-2})$$

For a reflection from the i -th interface, the last two square-roots in equation (C-1) yield unity. It is fortunate that the transformation of q is independent of the beam width, thus enabling us to compute the necessary reflection and transmission correction as a simple by-product of the ray tracing. Equation (C-2) has been derived under the assumption, that the radius of curvature of the interface is much larger than the width of the beam. Under this constraint, our final expression for multiply reflected or transmitted Gaussian beams is:

$$U(O_s) = U_0 \cdot \sqrt{\frac{v(O_s)}{v(O)}} \sqrt{\frac{q(O)}{q(O_s)}} \cdot \prod_{i=1}^n \left(R_i \sqrt{\frac{v(P_i^-)}{v(P_i^+)}} \sqrt{\frac{\cos(\alpha_i^+)}{\cos(\alpha_i^-)}} \right) . \quad (\text{C-3})$$

Unlike the classical ray-theoretical amplitudes, this expression involves two complex variables $q(O_s)$ and $q(O)$. The reflection or transmission coefficient R_i at the i th interface for acoustic pressure waves can be evaluated by assuming the continuity of both pressure and the normal component of particle velocity across an interface (Brekhovskikh, 1960).

END

**DATE
FILMED**

12/15/93

